RESEARCH AND APPLICATION ON THE MECHANICAL CHARACTERS OF ROTARY STEERING DRILLING TOOL

A Thesis

by

SHAN JIANG

Submitted to the Office of Graduate and Professional Studies of
Texas A&M University
in partial fulfillment of the requirements for the degree of

MASTER OF SCIENCE

Chair of Committee,	Jerome Schubert
Committee Members,	Maria A. Barrufet
	Robert H. Lane
Head of Department,	A. Daniel Hill

December 2014

Major Subject: Petroleum Engineering

ABSTRACT

Rotary steerable drilling tool systems (RSS) are ideal for tool integrating downhole automation control and drilling technology, which are used for drilling directional and complex track wells. A simply supported beam model is generally used to research bit side force for point-the-bit RSS tools. The greatest advantage is simplification in the analysis of the bit side force. However, for the side force solution on a point to the bit conditions, the existing literature ignore that this drilling tool system has an outward extended distance. Otherwise the bit in contact with the well wall will form a new support. According to the situation, a point to the bit tool has an outward extended distance; if we ignore this extended distance, and simplify it or just take it as the reaction force of the tool lower bearing support, or side force of the bit a great inaccuracy error will result. Because the beam has an outward extended distance related to the real bit side force, we need more research in this area.

Using to the principle of minimum complementary energy, we can explore the mechanical properties of rotary steerable tools. The rotary steerable tool mandrel force model is based on the mandrel and the rotary steering drilling tool which has three supports; upper and lower bearing and continuous beam model bit. The coordinate system is built in accordance with axial line of orienting rotary steerable drilling tool. The conclusions from the theory analysis and project example calculation in this paperindicate:

RSS technology is a powerful tool for oil exploration and development. It effectively solves technical difficulties in oil and gas exploration and development. Particularly, with regard to higher productivity and fewer drilling risks and downhole accidents with more exposed reservoirs, it delivers excellent performance.

A basic theoretical study of a rotary steering tool system helps us further master the mechanical characteristics of the tool system from the angle of mechanical behavior and features of the tool. In combination with different whipstocking operation principles, we have established different mechanical models to solve the mechanical property parameters, then we can assess the mechanical properties of the RSS.

DEDICATION

I'd like to thank my parents, for their love, unselfish encouragement and support.

ACKNOWLEDGEMENTS

I'd like to express my sincere thanks to all those who have lent me hands in the course of my writing this paper.

I would like to extend my sincere gratitude to my supervisor, Dr. Schubert, who has given me insightful guidance and useful suggestions on my thesis. I would like to thank my committee members, Dr. Barrufet and Dr. Lane, for their valuable comments and discussions. I would like to express my heartfelt gratitude to Dr. Walter, who has given me useful advice on my writing and has tried his best to improve my paper.

TABLE OF CONTENTS

Page

ABSTRACT ii

DEDICATION iv

ACKNOWLEDGEMENTS v

TABLE OF CONTENTS vi

LIST OF FIGURES viii

LIST OF TABLES x

1. INTRODUCTION 1

1.1 Difficulties and Challenges Facing the Drilling Technology of the Petroleum Industry in the 21st Century 1
1.2 Focus of Studies in Mechanical Behavior Characteristics of Rotary Steering Drilling Technology 4
1.3 Study Contents and Significance in Practice 6

2. BACKGROUND AND CHARACTERISTICS OF ROTARY STEERABLE DRILLING TOOL SYSTEMS (RSS) TECHNOLOGY 8

2.1 Main Features of Baker Hughes AutoTrak Rotary Steering Drilling Tool 10
2.2 Main Features of Schlumberger PowerDriver RSS 14
2.3 Main Features of Halliburton's Geo-Pilot Rotary Automatic Steering Tool 19

3. MECHANICAL CHARACTERISTICS OF RSS 26

3.1 Research on the Mechanical Characteristics for the Principle of Minimum Complementary Energy Mechanical Model 26
3.1.1 Some questions 26
3.1.2 Build up the mechanical model and solution 27
3.1.3 Analysis and discussion 35
3.1.4 Conclusions 37
3.2 Research on the Mechanical Characteristics of the Point-the-bit RSS 38
3.2.1 Problems 38
3.2.2 Mechanical model establishment 38

3.2.3 Analysis and discussion 44
3.2.4 Case study 47
3.2.5 Conclusions 50
3.3 Flexural Distortion Analysis of the Mandrel in an Orienting RSS 55
3.3.1 Introduction 55
3.3.2 Mechanical model 56
3.3.3 Discussion 61
3.3.4 Case studies 62
3.3.5 Conclusions 63
3.4 Research on the Mechanical Properties and Design Methods of Point-the-bit Rotary Steerable Drilling Tools 65
3.4.1 Issues raised 66
3.4.2 Point-the-bit rotary steerable drilling tool mandrel mechanics model 67
3.4.3 Analysis and understanding 79
3.4.4 Conclusions 81

4. ELASTIC STABILITY QUESTION ON TWO-SPAN CONTINUOUS BEAMS 83

4.1 Research on Elastic Stability of Compressed Bar for Two-Span Continuous Beams and Its Application in the Rotary Steerable Drilling Tools 83
4.1.1 Problems 83
4.1.2 Mechanic model establishment 84
4.1.3 Solutions and case studies 92
4.1.4 Calculations 95
4.1.5 Conclusion and reorganization 97

5. CONCLUSIONS 99

NOMENCLATURE 102

REFERENCES 104

LIST OF FIGURES

Page

Figure 2.1 Autotrak RCLS Downhole Steering Tool System Structure 10

Figure 2.2 Autotrak Rotary Steering Tool Working Principle 11

Figure 2.3 PowerDriver Rotary Steering Drilling System Structure 14

Figure 2.4 PowerDriver SRD Steering Principle 15

Figure 2.5 Hydraulic Disc Valve Structure 17

Figure 2.6 Geo-Pilot Rotary Steering Drilling System Structure 20

Figure 2.7 Geo-Pilot Rotary Steering Drilling Tool Working Principle 20

Figure 2.8 Geo-Pilot Structures 21

Figure 2.9 Relative Position Relations of Two Eccentric Rings 22

Figure 2.10 Geo-Pilot Working Principles 24

Figure 3.1 Point the Bit Rotary Steering Drilling Tool 27

Figure 3.2 Mechanical Model of Rotary Steering Drilling Tool 28

Figure 3.3 Mechanical Model of Case 1 31

Figure 3.4 Mechanical Model of Case 2 32

Figure 3.5 Mechanical Model of Case 3 34

Figure 3.6 The Relationship between Reaction Force and Distance AP 36

Figure 3.7 The Relationship between Reaction Force and Distance BC 36

Figure 3.8 Configuration of Point-the Bit Rotary Steerable Drilling Tools 39

Figure 3.9 Mechanic Models of Point-the Bit Rotary Steerable Drilling Tool 40

Figure 3.10 Relationship between Side Force and Distance c (When a=ℓ/4, b=3ℓ/4) ... 53

Figure 3.11 Relationship between Side Force and Distance c (When a=b=ℓ/2) 54

Figure 3.12 Relationship between Side Force and Distance c (When a=3ℓ/4, b=ℓ/4) ... 54

Figure 3.13 Schematic Diagram of Orienting Rotary Steerable Drilling Tool 56

Figure 3.14 Mechanic Model of the Mandrel in Orienting RSS 57

Figure 3.15 Relationship between Deflection and Bending Stress of Case 1 65

Figure 3.16 Point-the-Bit Rotary Steerable Drilling Tool Schematic Structure 66

Figure 3.17 Mechanical Model of Mandrel (Case 1)..... 68

Figure 3.18 Mechanical Model of Mandrel (Case 2)..... 68

Figure 3.19 Mechanical Model of Mandrel (Case 3)..... 70

Figure 3.20 Mechanical Model of Mandrel (Case 4)..... 72

Figure 3.21 Mechanical Model of Mandrel (Case 5)..... 75

Figure 3.22 Mechanical Model of Mandrel (Case 6)..... 77

Figure 4.1 Point-the-Bit Rotary Steerable Drilling Tool System 84

Figure 4.2 Configuration of Rotary Steerable Drilling System..... 85

Figure 4.3 Two-Span Continuous Beam Models with Same Intervals..... 86

Figure 4.4 Curve for Determing Minimum Root 94

LIST OF TABLES

Page

Table 3.1 Relationship between Reaction Force and Distance AP (assume ℓ=5)..... 35

Table 3.2 Relationship between Reaction Force and Distance BC (assume ℓ=5) 36

Table 3.3 Relationship between Side Force and Distance c (When a=ℓ/4, b=3ℓ/4) 52

Table 3.4 Relationship between Side Force and Distance c (When a=b=ℓ/2) 52

Table 3.5 Relationship between Side Force and Distance c (When a=3ℓ/4, b=ℓ/4) 53

Table 3.6 Relationship between Deflection and Bending Stress..... 64

Table 3.7 Dynamic Model in Different Condition 79

Table 3.8 Reaction Force in Different Condition 80

Table 4.1 Periodic Function Calculation in Case 1 91

Table 4.2 Periodic Function Calculation in Case 2 93

Table 4.3 the Critical Load for API Standard Drill Collar..... 98

1. INTRODUCTION

1.1 Difficulties and Challenges Facing the Drilling Technology of the Petroleum Industry in the 21st Century

Since the end of the 20th century, the petroleum industry has developed rapidly, especially in drilling efficiency and cost savings. Some drilling milestones in the 1990s were quite notable. For example, the combination of directional drilling services with adjustable stabilizers (Auto-Track) contributed greatly to the success of Extended Reach Drilling.

Wytch Farm oil field of Great Britain was drilled with extended reach wells from the shore into the offshore region, saving high offshore drilling costs. An offshore oil field was successfully developed, saving the cost of offshore islands and saved $150 million U.S. dollars of drilling cost. Sleipner oil field of the North Sea has extended reach wells instead of the original development plan, saving $1 billion U.S. dollars of development cost. Pedemales oil field of the U.S. used Extended Reach Drilling technology, saving $100 million U.S. dollars by eliminating drilling platforms.

Finally, offshore oil field XJ24-1 of China developed the nearby deposits through five extended reach wells, which saved high offshore platform construction costs and overcame many technical difficulties. The maximum horizontal displacement of Well A14 is up to 8,063 m. By 2002, comprehensive economic benefits had reached $327 million U.S. dollars.

Although we are making remarkable progress, the expansion of the world economy has given rise to escalating demands for petroleum, giving the industry new

challenges. For example, how can we develop new technologies to utilized more oil and gas resources with lower drilling costs? How can we improve the efficiency of directional drilling tools and operation safety on the basis of traditional directional drilling tools? How can we free ourselves from the confines of directional whipstocking techniques using elbows and a mud motor in directional drilling when using the rotary drilling to avoiding the risks of sticking and cutting bed resulting from slide drilling? These questions and challenges focus on directional drilling technologies and how to further improve the technology to better meet the energy demands of the world economy. Traditional drilling technologies, including directional drilling, mainly adopt motor-based directional drilling tools, which are unable to fully meet the requirements of the modern drilling. For this reason, RSS tools instead of traditional directional whipstocking tools were created.

Since the turn of the 21st century, drilling technology has turned to the development of automatic and intelligent drilling technologies. Baker Hughes AutoTrak, Schlumberger PowerDrive and Halliburton Geopilot are the most typical representatives of technical progress [1] [2]. The RSS has entered a large-scale industrial application stage, greatly advancing the progress of drilling technology. These tools mainly have the following technical characteristics: they combined drilling, electrical logging, information acquisition, transmission and control techniques. They progress from surface manual control to underground, fully automated, closed-loop control. They progress from surface-based intermittent information acquisition to underground direct and continuous information acquisition. All of which enable the discovery of

hydrocarbon reservoirs while drilling in a timely manner as well as reducing reservoir damage [3] [4] [5].

The key for the rotary steering drilling technology to move towards fully automated intelligent drilling is 3D well trajectory control drilling technology, centered on a closed-loop RSS. This is a leading technology of petroleum drilling engineering at present. Successful applications of RSS technology in horizontal wells, extended reach wells and highly-deviated wells have allowed enconomic devolop of multiple-target wells. These applications improved drilling speed, reduced accidents, and lowered drilling costs. Rotary steering, closed-loop drilling technology is the way forward for controled drilling technology in the future. Continuous rotation of drill strings reduces friction, enabling longer horizontal displacement and higher extension capacity. Hole cleaning reduces sticking risk. The toolface is adjusted without tripping in or out, which improves drilling efficiency. Timely operational adjustments improves control precision, and an optimal weight on bit (WOB) value can be used to increase the rate of penetration (ROP) for the best performance of the bit during steering.

These advancements of drilling represent a breakthrough technologies and a revolution in the petroleum industry. They symbolize new levels of achievements in drilling technology, especially new progress in directional drilling, that have made a great contributions to the economic development and construction of oil fields.

1.2 Focus of Studies in Mechanical Behavior Characteristics of Rotary Steering Drilling Technology

The large-scale application of rotary steering drilling technology started at the end of last century. It is typified by Baker Hughes AutoTrak RCLS push-the-bit type, Schlumberger Power Driver SRD modulation type, and Halliburton Geo-Pilot point-the-bit type technologies [6] [7]. Its most striking characteristic is the combination of mud-pulse measurement while drilling (MWD) technology and deflecting tools for directional drilling, with higher build-up rate that may be as great as 6. 5°/30 m to 8. 5°/30 m. The outer barrel can fully rotate (power drive) in such a way that the tool operation is more efficient, with better safety performance and less sticking. Thanks to the improvements in tool system performance, there were many successful cases of oil field development using RSS.

Great efforts have been made to develop electronic measurement technology for the tool system and to improve its control technology. To solve these problems, new steering drilling tools must be developed. Many applications verify that the RSS, as a new directional drilling tool, has superior performance. However, in terms of practical engineering applications, we still have much theoretical work to do to improve the RSS. Fundamental, studies of basic theory are needed, as well. We need to advance the point-the-bit type RSS to systematically improve the mechanical properties and dynamic characteristics. The following are some approaches suggested to address these needs.

1. Studies are needed of mechanical properties of point-the-bit RSS, including the acting forces produced by the biased load on mandrel and their influences on the

change of mechanical properties of bearings at upper and lower supports and on the tool lift.

2. Through current studies of the mechanical model and deflection deformation equation of point-the-bit RSS, we should treat the mandrel as one simply supported beam or an overhanging beam with two-point support or a mechanical model with three-point support. We must determine which method is closest to the actual situation. This is a major decision that must be made.

3. We need to studies of the mechanical properties of RSS from the statics field. We must assess the natural vibration frequency and its dynamic characteristics. This natural frequency study could clarify the resonant frequency of the tool system. So that, in operations, we could effectively prevent resonance of the tool system that may cause damage to the point-the-bit RSS [8].

Considerable previous research has been conducted on the drill string system and the method of adjusting the string stabilizer used for changing the bit side force [9]. This research focused mostly on the mechanical properties of bottom hole assembly (BHA) [10]; RSS studies were needed to explore the mechanical properties of the tool itself, to make significant advances in the technology.

1.3 Study Contents and Significance in Practice

Drilling engineering is a very practical, applied discipline. New tools and techniques are developed constantly. To design and ensure success of the new tools, we need to clearly define and understand new engineering technologies both in practice and theory. This research had three objectives.

The first, objective of our study of mechanical properties of rotary steering drilling tool is to understand the mechanical properties and structural design of the tool, to improve the mechanical structure in the working state. The goal is to ensure that the tool has strong deflecting capacity to allow necessary adjustments to the structure of RSS. But for longer system life, we must also consider whether the stress state at each supporting point is reasonable. Therefore, the tool's structural optimization and design must be based on full understanding of the mechanical properties of the tool system.

The second, objective of this research was to analyze mechanical properties of different mechanical models of RSS in practical situations. Among the existing mechanical models, which is most suitable for our reality? For example, if we use the simply supported beam model, the modeling would be rather simple. It is easy to solve the deflection equations. If we use the overhanging beam model, both the equation-based description and the equation solving are complicated. We can also use the minimum complementary energy method to solve the mechanical properties of RSS. But which method is closer to the actual situation? The answer to these questions requires that we conduct further research, only when a reasonable mechanical model is built can we get

realistic results. Only with a reasonable mechanical model can we use the results of theoretical study to guide design and practice.

Owing to the complexity of system configuration, our rotary steering drilling tool has mechanical structure, electronic data storage and signal transmission units, all of which constitute a complex system integrating mechanical, electronic and automation control. This complex system results in high operating cost, so people expect stable performance and a longer operating life. Therefore, we must minimize the tool's vibration characteristics. In dynamics principles, any system has its natural frequency. The third objective of this research focuses on natural frequency in RSS and reasonable methods and appropriate drilling parameters to minimize the resonance and thus, avoid damage to the tool system. The approach to assessing the dynamics properties of the tool system was to study the tool's structure and composition from the dynamics point of view and to select a reasonable speed range on the basis of drilling parameters and distribution of natural frequency. These effectively prevent resonance and increase the tool's service life [11] [12].

Improvements of drilling technology require successful integration of engineering technology and automate control technology. The technical system for drilling changes daily in response to the demand for more and more applications. Our research needs to follow the trends, make innovative engineering adjustments, and strive for further breakthroughs in basic theory. This research dedicated to making new contributions to petroleum engineering technology.

2. BACKGROUND AND CHARACTERISTICS OF ROTARY STEERABLE DRILLING TOOL SYSTEMS (RSS) TECHNOLOGY

Traditional directional drilling mainly uses directional drilling tools that uses downhole motors and depends on elbows and mud motors to achieve well trajectory control. These tools have poor working performance and complex operation, and a lot of slide drilling that carries the risk of downhole accidents. Such tools mainly have the following shortcomings and weaknesses.

(1) Slide drilling occurs during the use of a downhole motor for steering. In slide drilling the string bends more than in rotary drilling, and there is high axial friction between the sidewall and the string, so that the weight is difficult to apply to the bit. In extended reach wells and horizontal wells, this situation is even more serious, because it will cause string yielding in extreme cases. It limits the depth of horizontal and highly deviated wells.

(2) Conducting azimuth correction for a downhole motor from the surface, the rotary friction, torque on bit and torsional elastic deformation of drill pipes all hinder the toolface control. This affects the use of downhole motors in horizontal and highly deviated wells.

(3) In steerable drilling, the string's torsional elastic deformation gives rise to an unstable toolface angle, resulting in well trajectory distortion, which further increases friction forces on the string and also limits the drilling depth.

(4) Compared with rotary drilling, slide drilling makes cutting removal difficult and limits the ROP and drillable depth.

(5) Slide drilling has a lower ROP than rotary drilling. The downhole motor runs at a high speed, which decreases service life of the bit and the downhole motor and also increases the number of trips. Meanwhile, the use of downhole motors commonly causes bit sticking.

(6) Multiple shifts between slide drilling and rotary drilling may produce a large wellbore dogleg, which increases as the inclination curvature increases.

RSS technology is an important technical advance in automatic, intelligent drilling technologies, which is based on traditional directional drilling and is a leading method of petroleum drilling at present. It has the following characteristics: combined drilling, electrical logging, information acquisition, transmission and control techniques; progressing from surface manual control to underground full-automatic closed-loop control, from surface-based intermittent information acquisition to underground direct and continuous information acquisition. It is able to identify hydrocarbon reservoirs while drilling in a timely manner and drill in as many reservoirs as possible to improve per-well production.

Many countries have adopted the RSS technology in horizontal wells, extended reach wells, highly-deviated wells and 3D multiple-target wells, resulting in improved drilling speed, reduced accidents and lower drilling costs. Thanks to this technology, the string can continuously rotate with less friction, which enables longer horizontal displacement and higher extension capacity. Hole cleaning reduces the sticking risk and the toolface is adjusted without tripping in and out, which improves drilling efficiency. Timely adjustment of the drilling trajectory improves control precision, which increases

the rate of penetration (ROP) while meeting the needs of landing the well in the geologic target.

RSS have been put into industrialized application, greatly promoting drilling technology and oil field development and construction. Among the current rotary steering drilling technologies, Baker Hughes AutoTrak, Schlumberger PowerDrive and Halliburton Geopilot are the most representatives of mainstream technologies.

2.1 Main Features of Baker Hughes AutoTrak Rotary Steering Drilling Tool

Baker Hughes AutoTrak Rotary Steering Drilling System is a closed-loop drilling system [13]. Baker Hughes Inteq Autotrak RCLS is a push-the-bit type RSS. Autotrak RCLS RSS is shown in Figure 2.1.

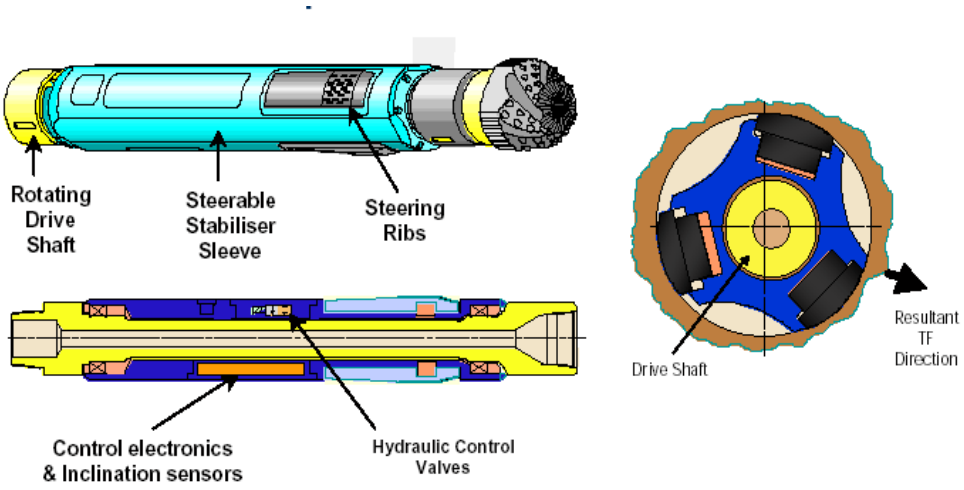

Figure 2.1 Autotrak RCLS Downhole Steering Tool System Structure

The AutoTrak downhole steering tool system is mainly composed of a non-rotating sleeve and a rotating drive shaft. The non-rotating sleeve provides rotational support for the rotating drive shaft via upper and lower bearings. There are drill strings and a bit respectively at top and bottom of the rotating drive shaft, which plays a role in transferring WOB, torque and drilling fluid. The non-rotating sleeve is equipped with a downhole CPU, measurement control, hydraulic system and biased actuator.

The steering principle of this system is shown in Figure 2.2. This tool has a unique non-rotating sleeve and an adjustable stabilizer, which nearly doesn't rotate compared with the rotating drive shaft of the drill bit; so, in rotary drilling, this non-rotating sleeve can stand relatively still to make sure the bit moves in a specific direction.

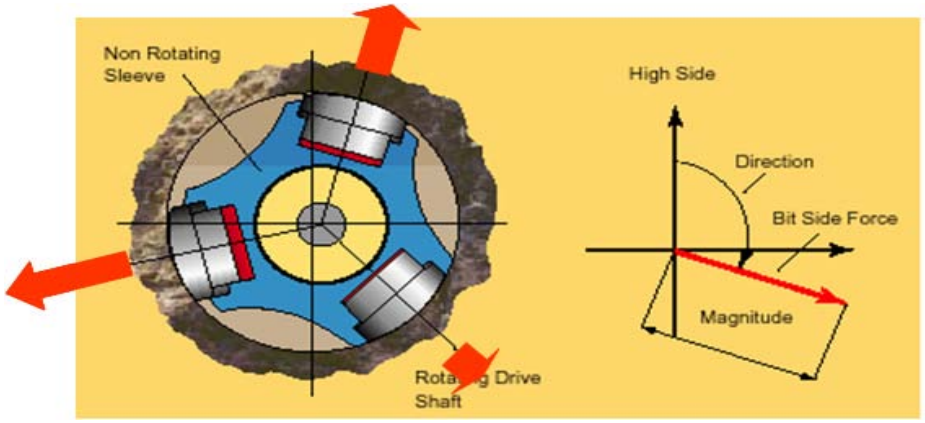

Figure 2.2 Autotrak Rotary Steering Tool Working Principle

When three steering ribs distributed uniformly in the circumferential direction are supported against the sidewall with different hydraulic pressures, respectively, this stops the non-rotating sleeve from rotating with the string; at the same time. The

counter-acting force from the sidewall will produce a biased resultant force on the downhole biased steering tool. Through controlling the magnitude of output hydraulic pressures of these three steering ribs, we can control the magnitude and direction of biased forces to control the steering drilling. The strength of hydraulic pressure is adjusted by the downhole CPU controlling the downhole control system. Before the downhole CPU is run into the well, well trajectory data are preset for it. Downhole operations can be compared to Measure While Drilling (MWD) well trajectory information or Logging While Drilling (LWD) with the design data to automatically control the hydraulic pressure. Also we can adjust the design parameters from the ground to control the hydraulic pressure, so as to realize the steering drilling.

The non-rotating sleeve rotates with different WOB or speed, 2 to 3 times every half an hour. For this reason, an electronic detector is set to measure the relative position of the non-rotating sleeve at any moment. Then the downhole CPU is run to adjust the pressure inside each piston. In this way, hydraulic steering forces are adjusted accordingly as the non-rotating sleeve rotates, to make sure the magnitude and direction of guiding forces will not be affected and the bit goes forward along the designated direction. During drilling, this system can be set in two drilling modes.

(1) Hold Mode. In this mode, the well trajectory is kept at an inclination and azimuth. It sets three parameters in the downhole CPU; Angle building/drop force, azimuth change force, and inclination/azimuth. If the well trajectory deviates from the preset inclination or azimuth, the downhole CPU will use the set angle building force to correct the well trajectory until the preset inclination and azimuth are restored. Setting of

the angle building force and azimuth change force is mainly to control the wellbore dogleg. In Hold Mode, angle building force and azimuth change force can be applied simultaneously.

(2) Steering Mode. This drilling mode is like the slide drilling method using a steerable motor, and can control the well trajectory. The magnitude and direction parameters of the resultant force vector produced by steering ribs must be set. The direction is equivalent to the toolface angle of bent housing motor; and the magnitude is used to control the change rate of the well trajectory. Compared with the steerable motor, this rotary steering tool can control the well trajectory more accurately, and bit side force and wellbore doglegs are continuously controlled by the closed-loop system.

The AutoTrak rotary steering tool has the following characteristics:

(1) Continuous adjustment of inclination or azimuth in rotary drilling, and strong angle holding capacity that contributes to the drilling of long angle holding sections;

(2) Enabled automatic directional control to provide accurate geosteering and reservoir positioning;

(3) Direction adjustment by AutoTrak that refers to the gravitational high side. For a well with an inclination below 3°, AutoTrak has difficulty in calculating the location of the high side exactly, and the well cannot be sidetracked from the vertical interval in the specified direction;

(4) In rotary drilling, two-way communication can be achieved between the downhole tool and the ground system, and thus well trajectory is adjusted in real time;

(5) In steering, the toolface change should not be too large and the dogleg not too small, otherwise it is a waste of operation time.

(6) AutoTrak may be used together with a drilling fluid motor to provide the bit with higher power and reduce the wear of drill pipe and casing.

2.2 Main Features of Schlumberger PowerDriver RSS

Schlumberger PowerDriver [14] is also a push-the-bit type RSS. The PowerDriver RSS is shown in Figure 2.3.

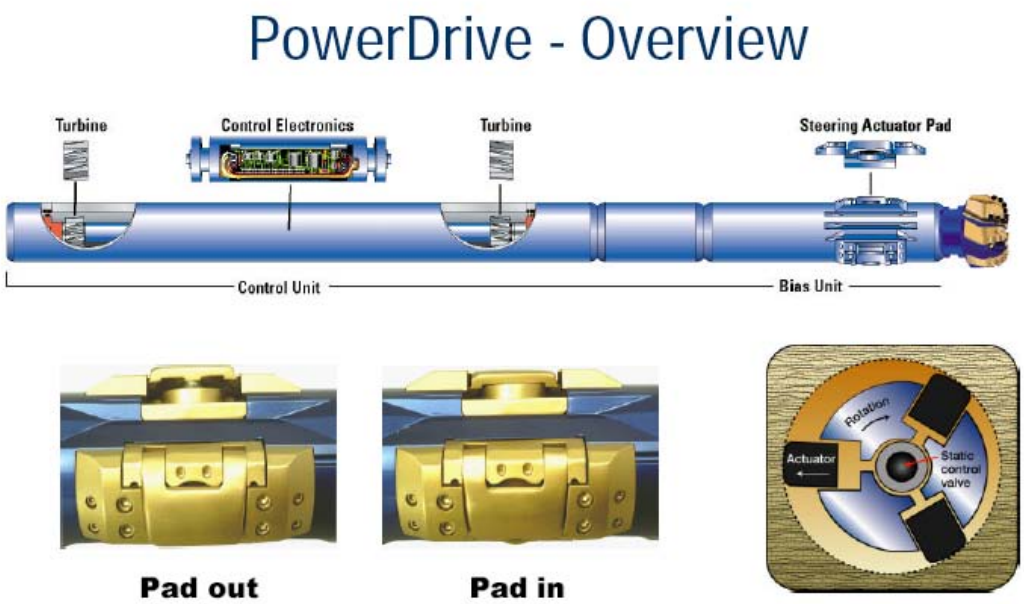

Figure 2.3 PowerDriver Rotary Steering Drilling System Structure

PowerDriver is composed of a stabilized platform and rib output in the control part, and the control mechanism. Its steering principle, similar to that of the Baker Hughes' Autotrak RCLS steering drilling tool, generates steering forces by use of the interaction between the expansion of the near-bit guide block and the sidewall, but it is structurally different. It excludes a static non-rotating sleeve and the three ribs rotate with the string. Its control unit, rotating directional valve and measuring mechanism are located in the middle of the string, and may remain relatively still. A Rotating directional valve can rotate to any position, which is the steering principle. The steering principle of PowerDriver SRD is shown in Figure 2.4.

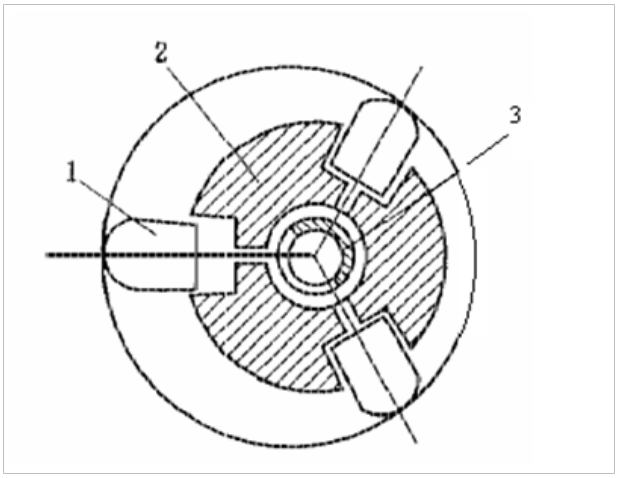

Figure 2.4 PowerDriver SRD Steering Principle

This tool has a self-stabilizing drilling fluid power and a seal control unit. It observes and controls the stabilized platform by rotation and adjusts the hole direction simultaneously. When steering is needed in one direction, each of the three guide blocks,

which are distributed uniformly in the circumferential direction rotates with the string. They may protrude in this direction once per rotation under the action of hydraulic pressure applied by the control system. This generates steering forces by pushing against the sidewall. This dynamically generates one side force on bit to move away from this direction, as a way of changing the inclination and azimuth. After changing direction, the guide block automatically retracts.

The PowerDriver directional control system includes a stabilized platform, hydraulic disc valve mechanism and guide block. The stabilized platform is located in the tool center by means of support bearings, and can freely rotate. It is connected via a connector to a hydraulic disc valve, and the direction is monitored by the internal sensor. At both upper and lower ends of the stabilized platform, one permanent magnetic turbo-alternator is installed and supplies power to the sensor and control circuit. The permanent magnet is embedded in the internal cavity of the turbine rotor. The motor coil rotates with the stabilized platform. The upper turbine rotates anticlockwise, while the lower one rotates clockwise. When there is loop current flowing through the turbine generator, the upper and lower turbines act on an anticlockwise and clockwise electromagnetic torque, respectively, on the stabilized platform. By comparing the direction measured by the internal sensor with the required direction stored in the storage unit of the control system, it can be concluded that the rotation of the stabilized platform is controlled by adjusting the generator load control signal and the difference of torque of the upper and lower turbines. The anticlockwise torque generated by the rotating drilling spindle and transferred via support bearing as well as the friction torque of the

disc valve generated in the bias unit can be balanced by adjusting the generator load to achieve stability. The movement of the stabilized platform is controlled via surface software, and the internal auto-control of inclination and azimuth can also be done programmatically.

The hydraulic disc valve mechanism consists of upper and lower disc valves. The upper disc valve is connected to the stabilized platform and rotates with it, whereas the lower disc valve is connected to the guide block and rotates with the external drill string. There is one fluid through hole in the upper disc valve, which can rotate in any direction before being arrested, so that only when the guide block rotates in one direction can it protrude. Hydraulic disc valve structure is shown in Figure 2.5.

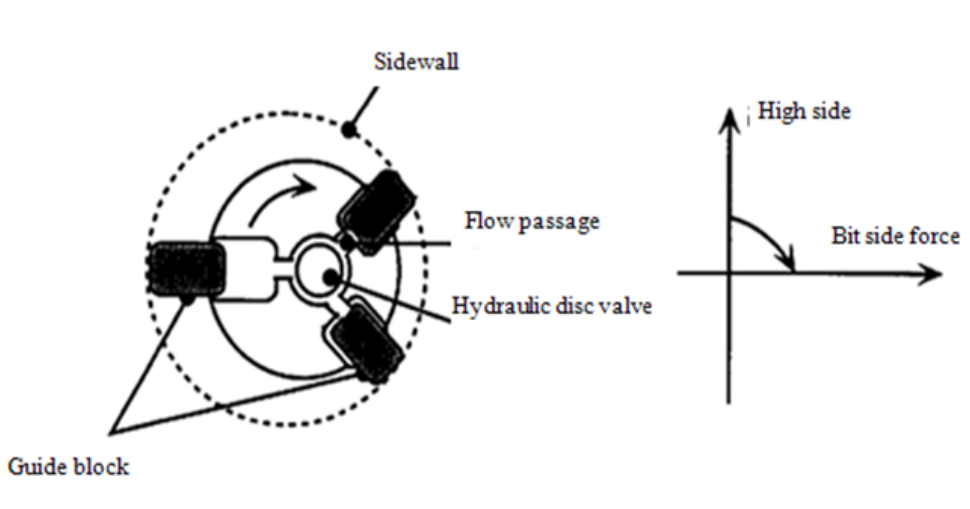

Figure 2.5 Hydraulic Disc Valve Structure

PowerDriver has the following functional characteristics:

(1) Steering in rotation further increases ROP and decreases sticking risks to make the borehole smoother, optimizing hole flushing and drilling parameters;

(2) Available for directional well, highly-deviated well, extended reach well and horizontal well;

(3) Sidetrack open-hole sections – with dogleg of 8 degrees/30 m

(4) Measure near-bit inclination and azimuth

(5) Available for 6”-18” holes

(6) Maximum pressure and temperature – 20,000psi 135℃

(7) Makes use of motor to drive PowerDriver to increase the torque and speed, further increasing ROP;

The relevant factors influencing PowerDriver performance are as follows.

(1) Mud density. It will affect bit pressure drop, so it is necessary to obtain the average value and possible range of the mud density on the next trip before PowerDriver is run into the well.

(2) Displacement. Before PowerDriver is run into well, it is necessary to obtain the available displacement range of mud pumps used by the drilling crew.

(3) Bit port. Calculated hydraulically using the above data. The bit port is selected according to the ideal working pressure drop of PowerDriver, if the total pumping pressure allows.

(4) Bit pressure stop. Bit pressure stop determines the magnitude of thrust block against sidewall. The mechanical part has a shorter life with excessive pressure

drop and might be damaged. The effect of PowerDriver is reduced with too small a pressure drop. Therefore, it is necessary to select an approprate value according to current well conditions. After the instrument is run into well, the bit pressure drop is often adjusted by changing the displacement.

(5) Rotary speed. If the speed is too low, it will not achieve the expected result. If too high, the mechanical parts will wear out more rapidly, depending on the current well conditions.

2.3 Main Features of Halliburton's Geo-Pilot Rotary Automatic Steering Tool

Halliburton's Geo-Pilot Rotary Automatic Steering Tool System [15] is also a non-rotating outer housing type steering tool. It is mainly composed of a rotating main shaft, a non-rotating outer housing, an eccentric cam unit, a cantilever bearing, and a focal bearing. Additionally, it includes control electronics and sensors packages, an eccentric cam unit drive mechanism, an anti-rotation device of the non-rotating outer housing, rotary dynamic seals and a pressure compensation system. The structure of Geo-Pilot system is shown in Figure 2.6.

Figure 2.6 Geo-Pilot Rotary Steering Drilling System Structure

But unlike AutoTrak and PowerDriver, Geo-Pilot does not use push-the-bit technology. The bias unit between the non-rotating outer housing and the rotating main shaft is used to bias the main shaft so as to provide the bit with a dip angle inconsistent with the borehole axis, thus resulting in steering. The working principle is shown in Figure 2.7.

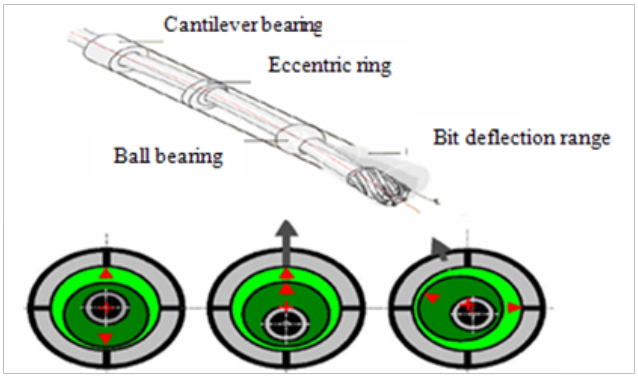

Figure 2.7 Geo-Pilot Rotary Steering Drilling Tool Working Principle

The system is mainly composed of a drive shaft, housing, drive shaft sealing device, non-rotating device, upper and lower bearings, eccentric device, near-bit deviation sensor, near-bit stabilizer, control circuit and sensors The Geo-Pilot structures is shown in Figure 2.8.

The drive shaft runs through the system, two ends of which are installed on bearings. The upper and lower parts are connected with the drilling tool and bit respectively and are the power transmission part of the system.

The housing is the system's outer tail structure, and does not rotate, relative to the formation. Its upper end is connected with the system's non-rotating device, and at its lower end there is one near-bit stabilizer.

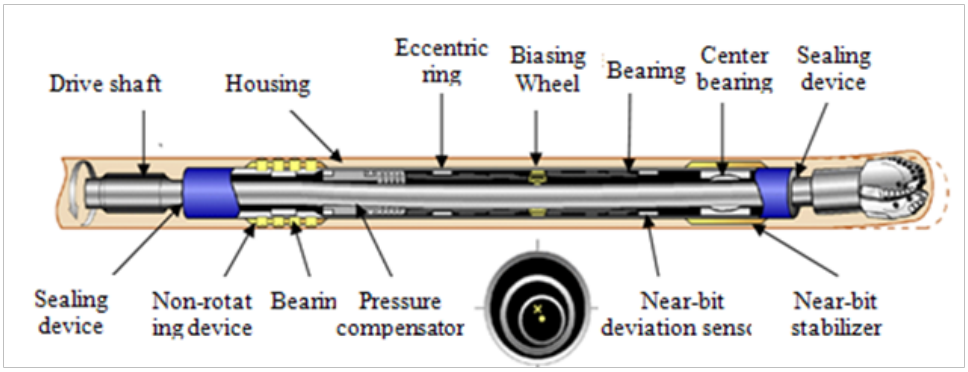

Figure 2.8 Geo-Pilot Structures

The winding of the non-rotating device becomes a flexible roller which ensures the stabilizer is fully packed and kept in touch with the sidewall, so that the system's housing does not rotate as the rotating shaft rotates.

The bearing consists of upper and lower parts. In addition to the conventional drag reduction, the upper bearing can prevent the drilling tool above the upper stabilizer from bending, where the lower bearing is mainly used to center the Geo-Pilot™ axis. It also acts as a pivot point, so that the bit can have better deflection when the drive shaft is slightly bent.

The eccentric device is the core of the steering system. It consists of two eccentric rings, and the mechanical devices controlling their movement are independent of each other. Its rotation direction and position are controlled by the control circuit. The rotating device is the shaft flanged with it. Relative position of two eccentric rings is illustrated in Figure 2.9.

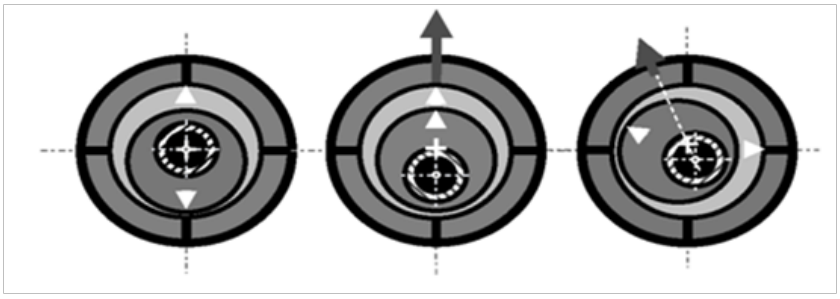

Figure 2.9 Relative Position Relations of Two Eccentric Rings

The control circuit and sensor are the heart of the tool steering systems. On one hand, the sensor constantly detects the system's toolface position (the toolface direction of the steering system). On the other hand, this part controls the steering system to correct the toolface deviation from the system in the drilling process according to the

designed toolface data, so that the system is always in a stable toolface position for construction.

The near-bit stabilizer mainly plays a supporting role to ensure that the bit is forced to change the axial direction when the drive shaft is bent, thus achieving bit orientation. The near-bit deviation sensor is used to measure the near-bit deviation and the system's toolface direction. The pressure compensator fixes the pressure inside rotary sealing position of the system slightly above the annular pressure.

The drive shaft of the Geo-Pilot RSS runs through the system, of which two ends are installed on bearings, and the upper and lower parts are connected with the drilling tool and bit respectively. It is a bit-driven power transmission unit. The system's housing is mounted on the bearing periphery, and does not rotate relative to the formation, providing a relatively stable toolface. The rotary sealing devices at both ends of the housing enable all moving parts to soak in the lubricating oil inside the housing while rotating the drive shaft, to reduce friction and protect these parts. Inside the housing, there is one sensor group that is used to measure near-bit inclination and the system’s toolface direction. The middle of the housing is the system’s core part, an eccentric device, which consists of two independent eccentric rings. When these two eccentric rings have opposite eccentric positions, the drive shaft does not bend. When they have the same eccentric direction, drive shaft bend is enhanced (giving strongest steering capacity).

When their eccentric positions are not aligned, the drive shaft’s bend is between the maximum bend amplitude and zero bend. This controls the system’s different

deflecting capacities. Eccentric direction can be achieved by controlling the rotation of the eccentric ring cam, and the eccentric direction vector sum can point to any direction within 360°. The vector sum's magnitude can also be adjusted between minimum and maximum, so that the system provides guidance in different directions and the deflecting capacity can be controlled between minimum and maximum.

When the two eccentric rings have different eccentric positions, the rotating shaft deflects. The degree and direction of deflection can be adjusted and controlled according to the driling needs. The system's eccentric device works with downhole control software, automatically preventing the system from working outside the range of design toolface error. The Geo-Pilot working principles are illustrated in Figure 2.10.

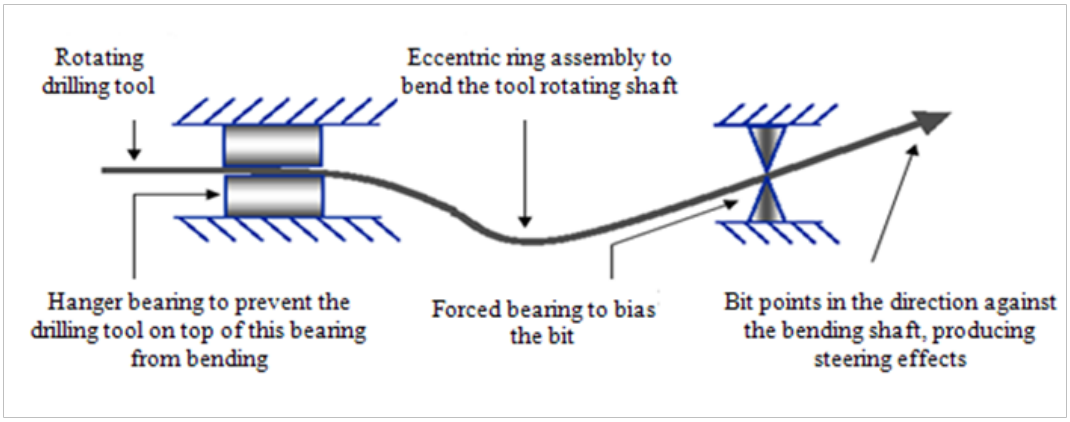

Figure 2.10 Geo-Pilot Working Principles

Geo-Pilot has the following advantages:

- Geo-Pilot has low friction, effectively keeps the trajectory extending forward. It can also be used without problems in both casing and logging operations after drilling is completed. Geo-PilotTM avoids bit side-cutting (bottom) and thus effectively reduces the tool vibration. This tool is especially applicable for construction of extended reach wells with high friction and high torque and 3D directional/horizontal wells with high complexity.
- Use of the system of construction is advantageous for eliminating borehole spirals and reducing borehole turns. It improves directional trajectory control effect, drilling efficiency and shortening the drilling period for casing and logging operations.
- Geo-Pilot has good hole cleaning, which reduces short trips and increases the rig's effective working hours to optimize the high angle hole effect.
- The extension of the extended bit is equivalent to the stabilizer effect, prolonging the bit service life.
- With longer bit life, the times required for tripping in/out is reduced and more time is spent in drilling, so ROP per well is increased.
- With use of extended gauge bit, the vibrations of downhole drilling tools as well as the probability of failure arising from MWD/LWD are reduced.
- Lithium batteries are used for power supply, instead of a turbine generator, which increases running reliability of the system and prolongs its effective working life.
- Systems isolation from mud eliminates the incompatibility of the system's bearings, seals and other mechanical parts with the mud.

3. MECHANICAL CHARACTERISTICS OF RSS

3.1 Research on the Mechanical Characteristics for the Principle of Minimum Complementary Energy Mechanical Model

Using to the principle of minimum complementary energy, we will explore the mechanical properties of rotary steerable tools. The rotary steerable tool mandrel force model is based on the mandrel and the rotary steering drilling tool which has three supports; upper and lower bearing and continuous beam model bit.

3.1.1 Some questions

Point-the-bit RSS in directional drilling have evolved rapidly in recent years. This system is characterized by a high build-up rate, and the ease of building up in shallow, unconsolidated formations. Therefore this system has gradually becomes representative of RSS technology and was widely welcomed by operators [16]. Now, the main systems in use are push-the-bit RSS and point-the-bit RSS. Schlumberger, Halliburton, Baker Hughes and Weatherford currently run and manufacture rotary steerable systems.

Much research has been done on going on the rotary steering drilling tool. This research work on the mechanical characteristics of the RSS has been widely reported [17] [18] in the literature. Double support conditions, explores the deformation equation of beam and dynamic characteristics.

However, for the side force solution on a point to the bit conditions, the literature [18] ignores that this drilling tool system has an outward extended distance. Otherwise the

bit in contact with the well wall will form a new support. In this content, further research is required.

According to the situation, a point to the bit tool has an outward extended distance; if we ignore this extended distance, and simplify it or just take it as the reaction force of the tool lower bearing support, or side force of the bit a great inaccuracy error will result. Because the beam has an outward extended distance related to the real bit side force, we need more research in this area.

3.1.2 Build up the mechanical model and solution

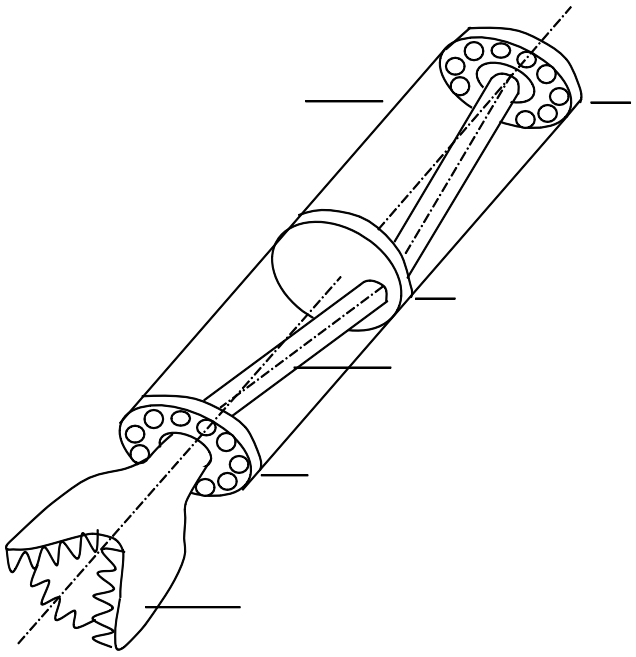

Figure 3.1 Point the Bit Rotary Steering Drilling Tool

The structure of point-the-bit RSS is shown in Figure 3.1. The major parts of a directional type point-the-bit RSS consists of the bit, below bearing support, mandrel, bias wheel, upper bearing support, shell etc. Its main working principle is that under the effect of the bias wheels, the mandrel is subject to flexure and deviating force on bit R_C. In this way the side forces on the bit can be created.

(1) Treat upper bearing support as fixed support

(2) Treat the force on bias wheel as concentrate load

(3) Consider the hole size as normal size.

The coordinate system is built in accordance with the axial line of the orienting RSS. Based on the assumptions above, the mechanic model of a mandrel is indicated as Figure 3.2.

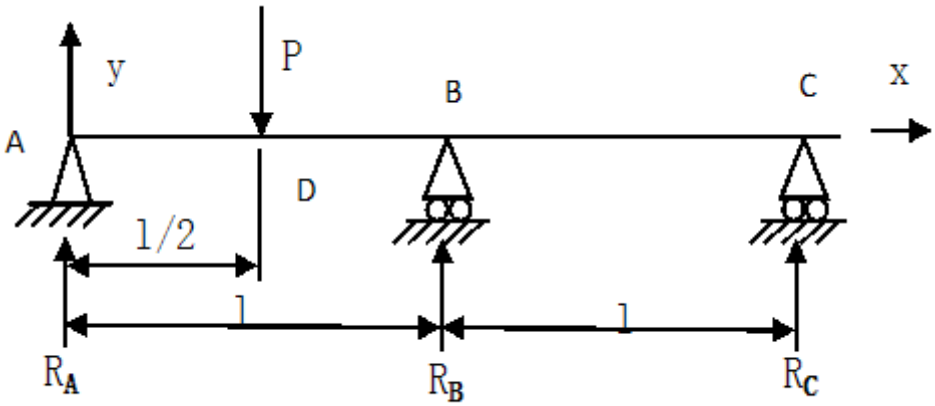

Figure 3.2 Mechanical Model of Rotary Steering Drilling Tool

From figure 3.2, we can combine R_C, the force on the below bearing support R_B and on the upper bearing support R_A which is made up of statically indeterminate system. We had one redundant reaction, so we treat R_A as redundant reaction, according to the static equilibrium condition, we got:

1. The force moment on C: $M_C = 0, 2R_A l + R_B l = \frac{3}{2} Pl$

$$\therefore \mathrm{R_B} = \frac{3}{2}\mathrm{P} - 2\mathrm{R_A} \tag{3.1}$$

2. The force moment on B: $M_B = 0, R_A l = \frac{Pl}{2} + R_C l$

$$\therefore \ \mathrm{R_C} = \mathrm{R_A} - \frac{\mathrm{P}}{2} \tag{3.2}$$

3. The moment equation on beam:

Section AD: $\mathrm{M_1} = \mathrm{R_A x}$ (3.3)

Section AB: $M_2 = R_A x - P(x - \frac{l}{2})$ (3.4)

Section AC: $M_3 = R_A(2l - x) + P(\frac{x}{2} - l)$ (3.5)

4. The deformation energy to the hole beam [19]:

$$u = \frac{1}{2EJ}\int \boldsymbol{M}_x^2 dx \tag{3.6}$$

$$\therefore u^* = \frac{1}{2EJ}\{\int_0^{\frac{l}{2}} \left(\boldsymbol{R}_A x\right)^2 dx + \int_{\frac{l}{2}}^{l}\left[\boldsymbol{R}_A x - P\left(x - \frac{l}{2}\right)\right]^2 dx + \int_l^{2l}\left[\boldsymbol{R}_A(2l - x) + P\left(\frac{x}{2} - l\right)\right]^2 dx\} \tag{3.7}$$

5. from the principle of minimum complementary energy in theory of elasticity

$$\pi^* = u^* - L^*$$

Due to bearing support no displacement

$$\therefore L^* = 0$$

$$\therefore \pi^* = u^*$$

6. Partial differential equation (3.7)

$$\frac{\partial \pi}{\partial R_A} = \frac{1}{2EJ}\left\{\int_0^{\frac{l}{2}} 2R_A x^2 dx + \int_{\frac{l}{2}}^{l} 2\left[R_A x - P\left(x - \frac{l}{2}\right)\right] x dx + \int_l^{2l} 2\left[R_A(2l-x) + P\left(\frac{x}{2} - l\right)\right](2l-x)dx\right\} = 0 \quad (3.8)$$

Integral calculation to equation (3.8):

$$R_A = \frac{13P}{32} = 0.41P \quad (3.9)$$

Applying equation (3.9) to equation (3.1):

$$R_B = \frac{11P}{16} = 0.69P \quad (3.10)$$

Applying equation (3.10) to equation (3.2):

$$R_C = -\frac{3P}{32} = -0.09P \quad (3.11)$$

From above we got solution of statically indeterminate system, according to this principal, we can optimization the design on the reaction point D of concentrate load P and the mandrel outward extended distance in rotary steering drilling tool.

[Example 1].Assume concentrate load P on the l/2 of the beam l_{AB}, while l_{BC}=l/10. Find the change rule of reaction force R_A, R_B, R_C. The mechanical model of case 1 is shown in figure 3.3.

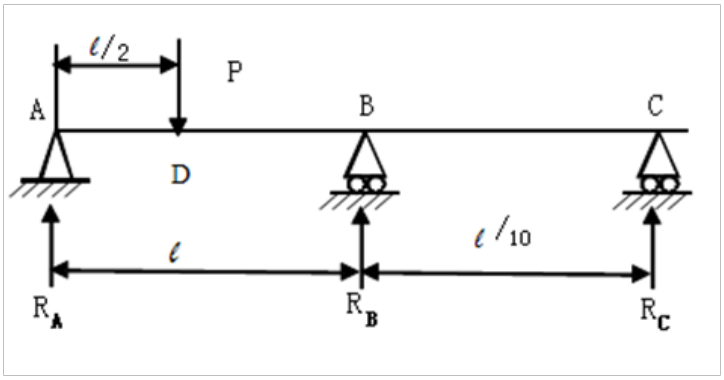

Figure 3.3 Mechanical Model of Case 1

Solution: From statics we got:

$$R_B = 6P - 11R_A \tag{3.12}$$

$$R_C = 10R_A - 5P \tag{3.13}$$

Each section bending of beam:

Section AD: $M_1 = R_A x$ (3.14)

Section AB: $M_2 = R_A x - P(x - \frac{l}{2})$ (3.15)

Section AC: $M_3 = R_A x + R_B(x - l) - P(x - \frac{l}{2})$ (3.16)

$\therefore$ Then the strain complementary energy of beam:

$$u^* = \frac{1}{2EJ}\left\{\int_0^{\frac{l}{2}}\left(R_A x\right)^2 dx + \int_{\frac{l}{2}}^{l}\left[R_A x - P\left(x - \frac{l}{2}\right)\right]^2 dx + \int_l^{\frac{11l}{10}}\left[R_A(11l - 10x) + P\left(5x - \frac{11}{2}l\right)\right]^2 dx\right\} \tag{3.17}$$

Partial differential equation (3.17)

$$\therefore \frac{\partial \pi}{\partial R_A} = \frac{1}{2EJ}\left\{\int_0^{\frac{l}{2}} 2R_A x^2 dx + \int_{\frac{l}{2}}^{l} 2\left[R_A x - P\left(x - \frac{l}{2}\right)\right] x dx + \int_l^{\frac{11l}{10}} 2\left[R_A(2l - x) + P\left(\frac{x}{2} - l\right)\right](2l - x) dx\right\} \tag{3.18}$$

Integrate equation (3.18):

$$R_A = \frac{29}{88}P = 0.33P \tag{3.19}$$

$$R_B = \frac{19}{8}P = 2.38P \tag{3.20}$$

$$R_C = -\frac{75}{44}P = -1.70P \tag{3.21}$$

[Example 2]. Assume concentrate load P on the 3l/10 of the beam l_{AB}, l_{BC}=l/10, Find the change rule of reaction force R_A, R_B, and R_C. The mechanical model of case 2 is shown in figure 3.4.

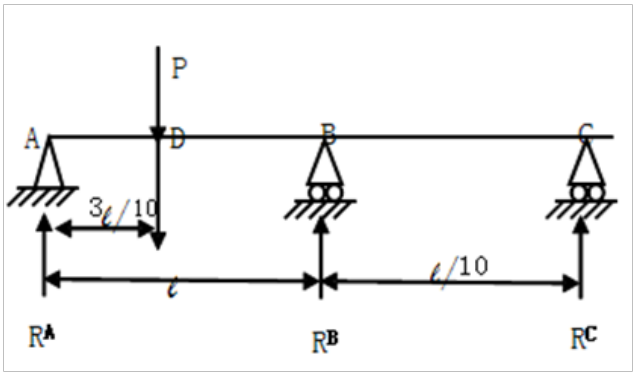

Figure 3.4 Mechanical Model of Case 2

Solution: From statics we got:

$$R_B = 6P - 11R_A \tag{3.22}$$

$$R_C = 10R_A - 7P \tag{3.23}$$

Each section bending of beam:

Section AD: $M_1 = R_A x$ (3.24)

Section AB: $M_2 = R_A x - P(x - \frac{3l}{10})$ (3.25)

Section AC: $M_3 = R_A x - P\left(x - \frac{3l}{10}\right) + R_B(x - l)$

$$M_3 = R_A(11l - 10x) + P(7x - \frac{77}{12}l) \tag{3.26}$$

$\therefore$ Then the strain complementary energy of beam:

$$u^* = \frac{1}{2EJ}\left\{\int_0^{\frac{3l}{10}}\left(R_A x\right)^2 dx + \int_{\frac{3l}{10}}^{l}\left[R_A x - P\left(x - \frac{3l}{10}\right)\right]^2 dx + \int_l^{\frac{11l}{10}}\left[R_A(11l - 10x) + P\left(7x - \frac{77l}{2}\right)\right]^2 dx\right\} \tag{3.27}$$

Partial differential equation (3.27)

$$\frac{\partial \pi}{\partial R_A} = \frac{1}{2EJ}\left\{\int_0^{\frac{3l}{10}} 2R_A x^2 dx + \int_{\frac{3l}{10}}^{l} 2\left[R_A x - P\left(x - \frac{3l}{10}\right)\right] x dx + \int_l^{\frac{11l}{10}} 2\left[R_A(11l - 10x) + P\left(7x - \frac{77}{10}l\right)\right](11l - 10x) dx\right\} = 0 \tag{3.28}$$

Integrate equation (3.28):

$$R_A = \frac{1307}{2200}P = 0.59P \tag{3.29}$$

$$R_B = -\frac{507}{200}P = -2.53P \tag{3.30}$$

$$R_C = -\frac{233}{220}P = -1.24P \tag{3.31}$$

[Example 3] Assume concentrate load P on the 7l/10 of the beam l_{AB}, while l_{BC}=l/10. Find the change rule of reaction force R_A, R_B, R_C. The mechanical model of case 3 is shown in figure 3.5.

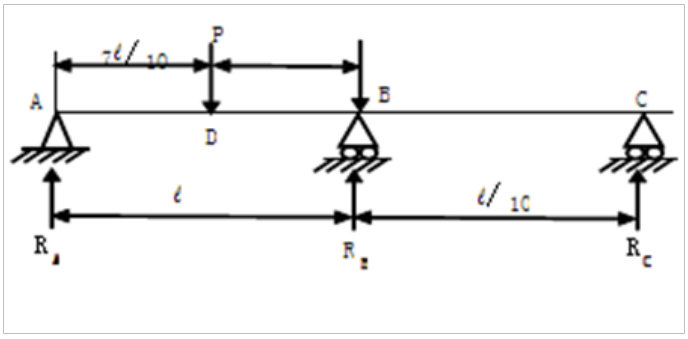

Figure 3.5 Mechanical Model of Case3

Solution: From statics we got:

$$\Sigma M_C = 0, \quad R_A \frac{11l}{10} + R_B \frac{l}{10} = \frac{4Pl}{10}$$

$$R_B = 4P - 11R_A \tag{3.32}$$

$$\Sigma M_B = 0, \quad \frac{l}{10} R_C + \frac{3l}{10} P = R_A l$$

$$R_C = 10R_A - 3P \tag{3.33}$$

Each section bending of beam:

Section AD: $M_1 = R_A x$ (3.34)

Section AB: $M_2 = R_A x - P\left(x - \frac{7l}{10}\right)$ (3.35)

Section AC: $M_3 = R_A x - P\left(x - \frac{7l}{10}\right) + R_B(x - l)$

$$M_3 = R_A(11l - 10x) + 3P\left(x - \frac{11}{10}l\right) \tag{3.36}$$

∴ Then the strain complementary energy of beam:

$$u^* = \frac{1}{2EJ}\left\{\int_0^{\frac{7l}{10}}\left(R_A x\right)^2 dx + \int_{\frac{7l}{10}}^{l}\left[R_A x - P\left(x-\frac{7l}{10}\right)\right]^2 dx + \int_l^{\frac{11l}{10}}\left[R_A\left(11l-10x\right)+3P\left(x-\frac{11l}{10}\right)\right]dx\right\}$$

Partial differential above equation

$$\frac{\partial \pi}{\partial R_A} = \frac{1}{2EJ}\left\{\int_0^{\frac{7l}{10}} 2R_A x^2 dx + \int_{\frac{7l}{10}}^{l} 2\left[R_A x - P\left(x-\frac{7l}{10}\right)\right]x dx + \int_o^{\frac{11l}{10}} 2\left[R_A\left(11l-10x\right)+3P\left(x-\frac{11l}{10}\right)\right]\left(11l-10x\right)dx\right\} \quad (3.37)$$

Integrate equation (3.34) $R_A = \frac{95}{2832}P = 0.03P$ (3.38)

$$R_B = \frac{10283}{2832}P = 3.6P \quad (3.39)$$

$$R_C = -\frac{289}{44}P = -6.56P \quad (3.40)$$

3.1.3 Analysis and discussion

From above result calculation, we get Table 3.1 and Table 3.2. The relationship between reaction force and distance AP is shown in Table 3.1 and Figure 3.6. The relationship between reaction force and distance BC is shown in Table 3.2 and Figure 3.7.

Table 3.1 Relationship between Reaction Force and Distance AP (assume ℓ=5)

No.	ℓ_{AP}	ℓ_{BC}	R_A P	R_B P	R_C P
1	1.5	0.5	0.59	-2.53	-1.24
3	2.25	0.5	0.33	2.38	-1.7
4	3.5	0.5	0.03	3.6	-6.56

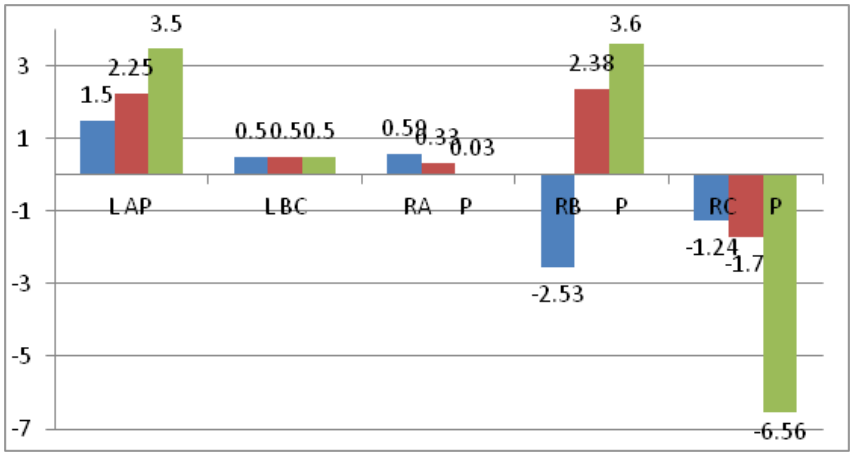

Figure 3.6 The Relationship between Reaction Force and Distance AP

Table 3.2 Relationship between Reaction Force and Distance BC (assume ℓ=5)

No.	ℓ_{AP}	ℓ_{BC}	R_A P	R_B P	R_C P
2	2.25	5	0.41	0.69	-0.09
3	2.25	0.5	0.33	2.38	-1.7

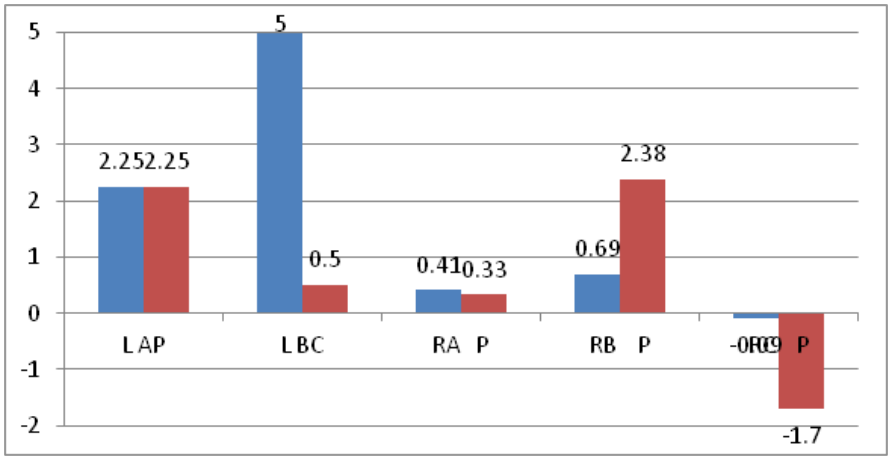

Figure 3.7 The Relationship between Reaction Force and Distance BC

From No.2 and 3, AP= l/2, due to different length of BC, when the length of BC decreased 90%, Rc will increased 18.8 times, that means if we want to have high build up rate, we need to decrease length of BC. When the length of BC= l/10, with the length of AP increased, Rc will increased from 1.24P to 6.56P. Rc will increase 4.3 times.

From table 3.1, we can obtain three recognize to improve the build-up force of the rotary steering drilling tool; First is to increase the concentration of bias force P. Second is the mandrel length of BC should be short; third is the location of P should be as closer as possible to the point B. They are three key points.

3.1.4 Conclusions

1. When researching the RSS, we focus on the mandrel. Using the beam statically indeterminate equation, according to the strain complementary energy of the beam and the principle of minimum complementary energy; we can easily solve the bearing reaction problems, such as side force on the bit.

2. The method proposed in the paper is the mechanical analysis of RSS. The deflecting force is related to three elements; the mandrel length l, outward extended distance l /n and location on the P.

3. When mandrel lengths are equal, the outward extended distance l_{BC} is shorter, the R_C is bigger and the l_{AP} is longer.

4. Use this research method, we can select and determine three design key points of the rotary steering drilling tool structural design. If we set the ideal R_C condition; we can get the P easily.

3.2 Research on the Mechanical Characteristics of the Point-the-bit RSS

3.2.1 Problems

Point-the-bit RSS accomplishes kickoff and trajectory controlling by the huge side force offered by axial deflection caused by bias devices as point loading enforcing axial deflection, which is decided by the structural characteristics of RSS.

A simply supported beam model is generally used to research bit side force for point-the-bit RSS tools. The greatest advantage is simplification, reaction at support can be obtained easily and it can approximate the bit side force. However, the real differences between them need further research.

3.2.2 Mechanical model establishment

The configuration of the tools is shown in Figure 3.8, have five parts as 1) axial shift; 2) tool housing; 3) upper bearing; 4) bias devices; 5) lower bearing. According to the force points of bit and axial shift, the mechanical model can be established as follows: 1) bias loads P; 2) reaction forcing at bit Q; 3) reaction force at upper and lower bearing;

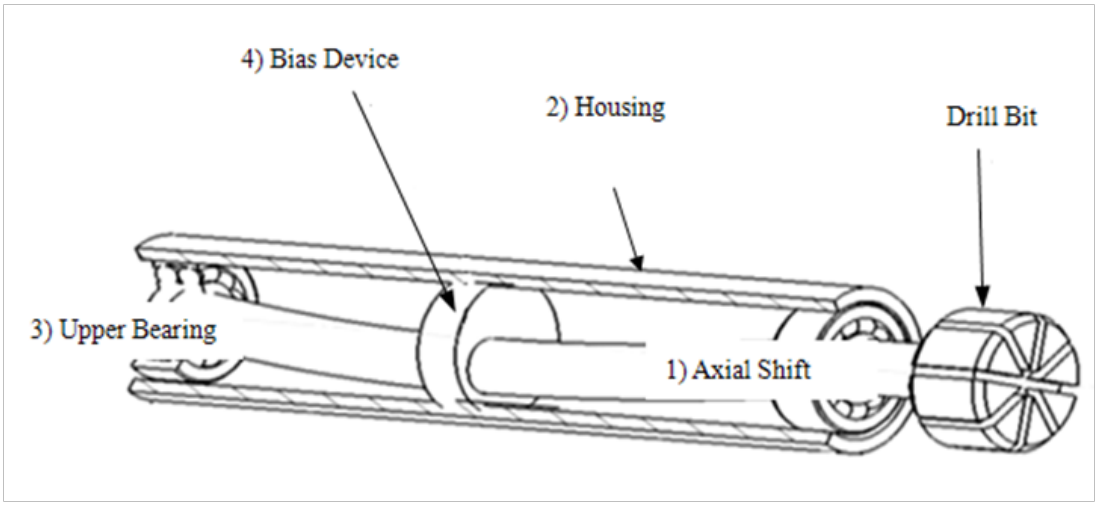

Figure 3.8 Configuration of Point-the-Bit Rotary Steerable Drilling Tools

Combined with real conditions onsite, and considering no weight-on-bit for axial shift of the tools, i.e. axial force is zero, and WOB is transferred to the drill bit by tool housing, it's own weight can be neglected because of the smaller size of the axial shift.

That is, no lateral uniform loading need be considered either. Therefore, a mechanical model of the tools can be established. This is a beam with overhang model that drill bit extension from lower bearing which is subjected to reaction force Q exerted by formation. The mechanic model of point-the-bit RSS is shown in figure 3.9.

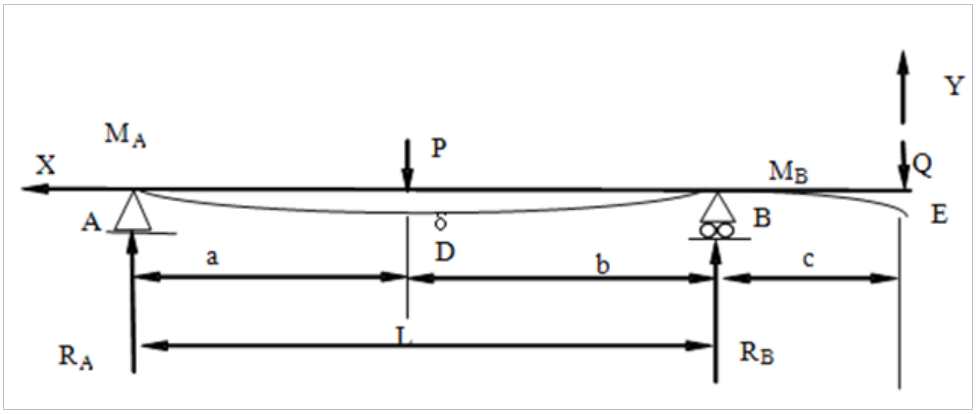

Figure 3.9 Mechanic Models of Point-the-Bit Rotary Steerable Drilling Tool

The Literature 2 shows that [20]

When $0 \le x \le c$, $EJy_1'' = M_1 = -Qx$ (3.41)

When $c \le x \le (b+c)$, $EJy_2'' = M_2 = -Qx + R_B(x-c)$ (3.42)

When $(b+c) \le x \le (l+c)$,

$$EJy_3'' = M_3 = -Qx + R_B(x-c) - P(x-b-c) \quad (3.43)$$

On the integration of equation (3.41) (3.42) (3.43), get equation (3.44) (3.45) (3.46)

$$EJy_1' = -\frac{Q}{2}x^2 + c_1 \quad (3.44)$$

$$EJy_1 = -\frac{Q}{6}x^3 + c_1 x + D_1 \quad (3.45)$$

$$EJy_2' = -\frac{Q}{2}x^2 + \frac{R_B}{2}(x-c)^2 + c_2 \quad (3.46)$$

$$EJy_2 = -\frac{Q}{6}x^3 + \frac{R_B}{6}(x-c)^3 + c_2 x + D_2 \quad (3.47)$$

$$\mathrm{E}Jy_3' = -\frac{Q}{2}x^2 + \frac{R_B}{2}(x-c)^2 - \frac{P(x-b-c)^2}{2} + c_3 \tag{3.48}$$

$$\mathrm{E}Jy_3 = -\frac{Q}{6}x^3 + \frac{R_B}{6}(x-c)^3 - \frac{P(x-b-c)^3}{6} + c_3 x + D_3 \tag{3.49}$$

Boundary conditions:

When $x = c$, $y_1 = y_2 = 0$ (3.50)

$$y_1' = y_2' \tag{3.51}$$

When $x = b + c$, $y_2 = y_3$ (3.52)

$$y_2' = y_3' \tag{3.53}$$

Therefore, we can get integration constants:

$$C_3 = C_2 = C_1 = EJ\theta_0 \tag{3.54}$$

$$D_3 = D_2 = D_1 = EJy_0 \tag{3.55}$$

And then, when $x = c$, $y_1 = 0$ (3.56)

$$x = l + c, \; y_3 = 0 \tag{3.57}$$

Substitute equation (3.56) into equation (3.45), then:

$$c_1 c + D_1 = \frac{Q}{6}c^3 \tag{3.58}$$

And substitute equation (3.54) and equation (3.55) into equation (3.49):

$$EJy_3 = -\frac{Q}{6}x^3 + \frac{R_B}{6}(x-c)^3 - \frac{P(x-b-c)^3}{6} + c_1 x + D_1$$

When $x = l + c$, from equation (3.57):

$$c_1 l + c_1 c + D_1 = \frac{Q}{6}(l+c)^3 - \frac{R_B}{6} l^3 + \frac{P}{6} a^3 \tag{3.59}$$

Substitute equation (3.58) into equation (3.59):

$$c_1 = \frac{1}{6l}\left\{Q\left[(l+c)^3 - c^3\right] - R_B l^3 + Pa^3\right\} \tag{3.60}$$

Substitute equation (3.60) into equation (3.58):

$$\mathrm{D}_1 = \frac{c}{6l}\left\{Q\left[lc^2 - (l+c)^3 + c^3\right] - R_B l^3 + Pa^3\right\} \tag{3.61}$$

Because rotating angle at point E is

$$\theta_E = \theta_0 = \frac{c_1}{EJ} = \frac{1}{6EJl}\left\{Q\left[(l+c)^3 - c^3\right] - R_B l^3 + Pa^3\right\} \tag{3.62}$$

In the coordination, rotating angle is clockwise direction, so rotating angle is positive.

$\because\ D_1 = EJy_0$

$$\therefore\ y_0 = f_E = \frac{D_1}{EJ} = \frac{c}{6EJl}\left\{Q\left[lc^2 - (l+c)^3 + c^3\right] - R_B l^3 + Pa^3\right\} \tag{3.63}$$

Supposing $x = b + c$ and substitute it into equation (3.49), deflection at midpoint can be derived:

$$EJy_3 = -\frac{Q}{6}(b+c)^3 + \frac{R_B}{6} b^3 + c_1 b + \frac{Q}{6} c^3 \tag{3.64}$$

$\because$

$$R_B = \frac{Pa + Q(l+c)}{l}$$

$$y_3 = \frac{1}{6EJl}\left\{Ql\left[c^3 - (b+c)^3\right] - Qb\left[c^3 - (l+c)^3\right] + \left[Pa + Q(l+c)\right]\left(b^2 - l^2\right)b + Pa^3 b\right\} \tag{3.65}$$

From the static of theoretical mechanics:

$$\sum M_A = 0\,,\ Pa + Q(l+c) = R_B l \quad R_B = \frac{Pa + Q(l+c)}{l} \tag{3.66}$$

$$\sum M_B = 0\,,\ Qc + R_A l = Pb \quad R_A = \frac{Pb - Qc}{l} \tag{3.67}$$

Let x=0, from equation (3.45) and equation (3.61): $EJy_1 = D_1$

From equation (3.63), we can get:

$$y_0 = \frac{c}{6EJl}\left\{Q\left[lc^2 - (l+c)^3 + c^3\right] - R_B l^3 + Pa^3\right\}$$

$$y_0 = \frac{c}{6EJl}\left\{Q\left[lc^2 - (l+c)\left[(l+c)^2 + l^2\right] + c^3\right] + Pa\left(a^2 - l^2\right)\right\}$$

Specially, considering deflection in wellborn at drill bit is nearly zero, therefore:

$$y_0 = 0\,,\ \text{and}\ \ Q\left[lc^2 - (l+c)\left[(l+c)^2 + l^2\right] + c^3\right] = Pa\left(l^2 - a^2\right) \tag{3.68}$$

Combine equation (3.65) and equation (3.68), we can get:

$$Q = \frac{6EJly_3\left(a^2 - l^2\right)}{b\left[a^2\left(b^2c - 3lbc + 6l^2 + 2lc^2 + 2l^3\right) + l^3\left(3bc - 6lc - 2c^2 - 2l^2\right) + b^2l\left(3lc + 2c^2 + 2l^2\right)\right]} \tag{3.69}$$

$$P = \frac{12EJy_3(l+c)^2 l^2}{ab\left[a^2\left(b^2c - 3lbc + 6l^2 + 2lc^2 + 2l^3\right) + l^3\left(3bc - 6lc - 2c^2 - 2l^2\right) + b^2l\left(3lc + 2c^2 + 2l^2\right)\right]} \tag{3.70}$$

Therefore, equation about the side force at drill bit P and bias loading Q has been derived by now, obviously, essential discussion concerning side force at bit and bias loading is needed in further.

3.2.3 Analysis and discussion

From equation (3.68), we could know how to calculate and evaluate build angle capability of the tools, this equation looks like complex, we cannot find the regulation of steering capability easily, therefore, we will discuss considering three cases:

When a=l/4, b=3l/4; that is, bias device located nearby the position of upper bearing, we can get from equation (3.69):

$$Q = \frac{640EJy_3}{l\left(153lc + 64c^2 + 64l^2\right)} \tag{3.71}$$

We can find that

(1) When the dimensions of the tool is fixed, E, J and l are known constant, if given bias device deflection y_3, steering capability of the bit is a function of c (distance between upper bearing and bit) and also is in proportion to E, J and deflection of axial shaft y_3. That is, buildup capability of the bit is increasing with extension length of the beam with overhang, and vice versa.

(2) When extension length c= l, from equation (3.71) we can know the bit steering force P_1.

$$Q_{1a} = \frac{2.28EJy_3}{l^3} \tag{3.72}$$

And when c= l/2, from (3.69), we can know bit side force P_2.

$$Q_{2a} = \frac{4.09EJy_3}{l^3} \tag{3.73}$$

From above, we can know

(1) When c is become shorter, Q will increase, and we can know from equation (3.71) and equation (3.72), when c shortened a half, Q will become 1.8 to 3.8 times of it before.

(2) With c shortened continuously with the rate of 50%, the rate of side force increased gradually decrease from 1.8 times to 1.1 times.

Above two findings show us if higher side force is desired, the shorter of extension length should be, however the extent should be appropriate, the tendency and characters see following table 3.3.

When a=b=l/2; we can get from equation (3.69):

$$Q = \frac{114EJy_3}{l\left(41lc + c^2 + l^2\right)} \tag{3.74}$$

When extension length c=ℓ, from equation (3.74) we can get bit side force Q_{1b}.

$$Q_{1b} = 3.34\frac{EJy_3}{l^3} \tag{3.75}$$

When extension length c=ℓ /2, from equation (3.73) we can get bit side force Q_{2b}.

$$Q_{2b} = 6.62\frac{EJy_3}{l^3} \tag{3.76}$$

We can find clearly that:

(1) The same regulation with case 1, that is with the shorter of c, the higher of side force;

(2) with movement of bias device position to middle of axial shaft, side force Q increase obviously, when c = ℓ, Q_{2b} will be two times greater than Q_{1b}, that is, coefficient of Q_{1b} is 3.34, will increase to 6.62, coefficient of P_{2b}, which is obviously;

(3) With the shorten of c and length ℓ with rate of 50%, side force Q increased 2 to 12 times than that of before, detailed see Table 3.4.

When a=3l/4, b=l/4 ; that is the position of bias device moved from the middle to the direction of the lower bearing, from equation (3.69) we could know side force calculation formula:

$$Q = \frac{2688EJy_3}{l\left(531lc + 192c^2 + 192l^2\right)} \tag{3.77}$$

Observation of above formula, we can find:

$$\text{When } c = l:\ Q_{1c} = 2.94\frac{EIy_3}{l^3} \tag{3.78}$$

$$c = l/2:\ Q_{2c} = 5.31\frac{EIy_3}{l^3} \tag{3.79}$$

Therefore,

(1) When c is become shorter, side force Q is greater;

(2) when a = 3 ℓ /4, its side force is greater than conditions that a is ℓ /4, however, is less than conditions that a = ℓ /2; we can find this regulations merely comparing the first item of the formula, when c equals to ℓ and a equals to ℓ /4 , Q_{1a} equals to $2.28EJy_3/\ell^3$, and when a = ℓ/2, $Q_{1b} = 3.34EJy_3/\ell^3$, when a = 3 ℓ /4 , $Q_{1c} = 2.9EJy_3/\ell^3$;

(3) We can find clearly that with the movement of side force point nearby the point A and B (direction of upper and lower bearing), the less of bit side force, only when the action point at the middle of the shaft, can we get the larger bit side force which we desired.

3.2.4 Case study

Example 1

Assumption: outer diameter of shaft OD is 9.5cm, inner diameter of shaft ID is 4.3cm, length of shaft ℓ is 300 to 600cm, when bias loading Q is exerted on the position of a = ℓ /4, and the length of BE section c decrease from ℓ /2 to ℓ /3, deflection y_3 change between 1 to 3 cm. Determine the side force Q and its changing regulations, E equals to 2.1×10^6kg/cm^2.

Solutions:

ℓ = 600cm, y3=1cm, c= ℓ /2

When a= ℓ/2, side force Q can be calculated from (3.71):

$Q=4.09*2.1*10^6*379*1/600^3=15.1$ Kg

When ℓ =500cm, a = ℓ/2, side force Q can be calculated from (3.71):

Q=26.1 Kg

Size force decreased with shaft length decrease, and will increased when ℓ= 600cm, c = ℓ /30,

(1) While side force Q=34.1kg, however, when ℓ= 300cm and c= ℓ /30, that is length of axial shaft ℓ decreased 50%, side force Q will increased from 34.1kg to 273kg at the position that c equals to ℓ /30, that means bit side force is 8 times than before.

(2) With decreasing of c, side force Q will increase, for example, we can find that when ℓ= 400cm, c =ℓ/2, Q= 50.9kg, while c = ℓ /20, Q =110.8kg, that is, when c becomes 0.1 times, side force will increase 2 times than before.

(3) Bit side force Q will increase with shaft deflection increasing, basic regulations is when deflection y_3= 2cm(increase 1cm), its side force will be 2 times than that of before at the same conditions, when deflectiony_3=3cm, the side force will be 3 times than before, when shaft length ℓ= 600cm, deflection y=1cm, side force Q will be 15.1kg, and if only change deflection while no change other conditions, we can find that, side force Q will be 30.2kg when y_3= 2 cm, however, side force Q become 45.3kg when deflection increased to y_3=3 cm, side force P increased greatly compared with the increasing of deflection.

Example 2

The position of bias loading P moved forward the middle of shaft that is when an equals to half of ℓ, and other conditions unchanged with example 1. Determine the bit size force and its changing regulations at this case.

Solution:

When ℓ equals to 600cm, y_2 equals to 1cm, and equals half of ℓ which is same as b, we can calculate the side force at this case by equation (3.73), detail processing is same with example 1, we can find:

With the movement of position of bias loading forward to middle of shaft, that is when a increased to 2 times than that of before, its side force rapidly increased, for an instance, when ℓ = 600cm, c = ℓ /30=20cm, a = ℓ /4, and the deflection y_3 = 1 cm, we can know the side force Q= 34kg, while deflection y_3 = 2cm, side force Q = 68kg. From Table 3.3 and Table 3.4, we can find that the side force Q is 224kg and 449kg at this case

when a = ℓ/2. that is, with a becomes 2 times than before (from ℓ /4 to ℓ /2), the side force will be 6.6 times as before, which illustrate that if higher side force desired, the position of bias loading should move forward to the middle of the shaft, while decrease c, which could increase the side force rapidly. Other characters are same with above, will not repeated here.

Example 3

When the position of bias loading P move forward to lower bearing continuously, that is when a =3ℓ/4, other conditions is the same, determine the side force Q and its changing regulations.

Solution:

When ℓ = 600cm, deflection y_3 is 1 cm and a = 3ℓ/4, we can calculate the side force Q by formula (3.77), we can find that:

With position of bias loading P moves forward to lower bearing direction, that is a becomes 3 times than that of before (a =3ℓ/4), when ℓ= 600cm, c= ℓ /30=20cm and deflection y_3=1cm, while when deflection y_3=2cm, side force Q= 94kg, and when deflection y_3=3cm, side force Q =142kg. In this case, side force Q decreased approximately 80% of the case that a equals half of ℓ, whic h reveal to us that position of bias loading P move from the middle of shaft, the side force decreased. Other characters are same, will not repeated here.

To sum up, we can get the formula for side force of point-the-bit rotary steerable drilling tools, and also can find its characters as follows:

(1) The bit side force of point-the-bit RSS is closely related with it dimension such as length, side force Q will be greater if shaft length is shorter, generally, from Table 3.3 to Table 3.5, we can find when shaft length decreased from 6cm to 3cm, the bit side force will increased 5 times to 8 times than that of before, if c is the same.

(2) Q is related with tools design and its structure, when position of P is in the middle of mandrel, Q is the biggest, we can find these phenomena in the solution, when a equals to half of ℓ, side force Q is greater than the cases when a equals to ℓ/4 and 3ℓ/4, and at the same conditions, side force when a equals to half of ℓ is 6.5 times than the case when a equals to ℓ /4, and is 4.7 times than the case when a equals to 3ℓ/4, details see Table 3.3 to Table 3.5. The relationship between side force and distance c are shown in Table 3.3, 3.4 and 3.5.

(3) Q is related the distance between bit and lower bearing, Q will be greater if c is shorter, when ℓ= 600 cm, 500 cm, 400cm respectively, if c equals to 40 cm and 20 cm, the ratio of Q under this two cases will be nearly 1.6 to 1.7 times, that is if c shortened from 40 cm to 20 cm, side force will increase 1.6 to 1.7 times than that of before.

(4) Q is in proportion to shaft deflection y, shaft dimension and polar moment of inertia, which can be found from formula (3.70), (3.73) and (3.76), no matter where the bias loading position is.

3.2.5 Conclusions

The methods in this paper reveal the mechanical characteristics of point-the-bit RSS and its regulations of side force. The mechanical model for beam with overhang can

help us better understand the tools mechanical characteristics and have great significant in guiding the tools structural design work.

Results from this paper show that when people design or select the point-the-bit RSS tools, if higher side force is desired, they should pay attention to the tools structural design. The tools mandrel length should be shorter, the distance between the bit and lower bearing should be shorter, and the position of bias loading should be at the middle of the mandrel, while, mandrel deflection should be as great as possible. These key parameters determine the side force, and then determine the steering capability of the tools. The relationship between side force and distance c are shown in Figure 3.10, 3.11 and 3.12.

The side force at different bias loading positions is calculated in this paper. These reveal that, when designing point-the-bit RSS tool, the bias device could be designed as moveable. This could meet the need of greater side forces when we put the bias device forward to the middle of the shaft. This can also reduce side force putting the bias device forward to both ends of the shaft when we want to drill a smooth hole.

Table 3.3 Relationship between Side Force and Distance c (when a=ℓ/4, b=3ℓ/4)

extension distance c	side force Q	increase of multiple for each	increase of multiple
c= ℓ	Q_{1a} = 2.28*E*J*y/ℓ^3		
c= ℓ/2	Q_{2a} = 4.09*E*J*y/ℓ^3	1.8	1.8
c= ℓ/4	Q_{3a} = 6.02*E*J*y/ℓ^3	1.5	2.6
c= ℓ/8	Q_{4a} = 7.6*E*J*y/ℓ^3	1.3	3.3
c= ℓ/16	Q_{5a} =8.67*E*J*y/ℓ^3	1.1	3.8

Table 3.4 Relationship between Side Force and Distance c (when a=b=ℓ/2)

extension distance c	side force Q	increase of multiple for each	increase of multiple
c= ℓ	Q_{1b} = 3.34*E*J*y/ℓ^3		
c= ℓ/2	Q_{2b} = 6.62*E*J*y/ℓ^3	2.0	2.0
c= ℓ/4	Q_{3b} = 12.7*E*J*y/ℓ^3	1.9	3.8
c= ℓ/8	Q_{4b} = 23.45*E*J*y/ℓ^3	1.8	7.0
c= ℓ/16	Q_{5b} = 40.39*E*J*y/ℓ^3	1.7	12.1

Table 3.5 Relationship between Side Force and Distance c (when a=3ℓ/4, b=ℓ/4)

extension distance c	side force Q	increase of multiple for	increase of
c= ℓ	Q1c = 2.94*E*J*y/ℓ^3		
c= ℓ/2	Q2c = 5.31*E*J*y/ℓ^3	1.8	1.8
c= ℓ/4	Q3c = 7.9*E*J*y/ℓ^3	1.5	2.7
c= ℓ/8	Q4c =10.28*E*J*y/ℓ^3	1.3	3.5
c= ℓ/16	Q5c =11.89*E*J*y/ℓ^3	1.2	4.1

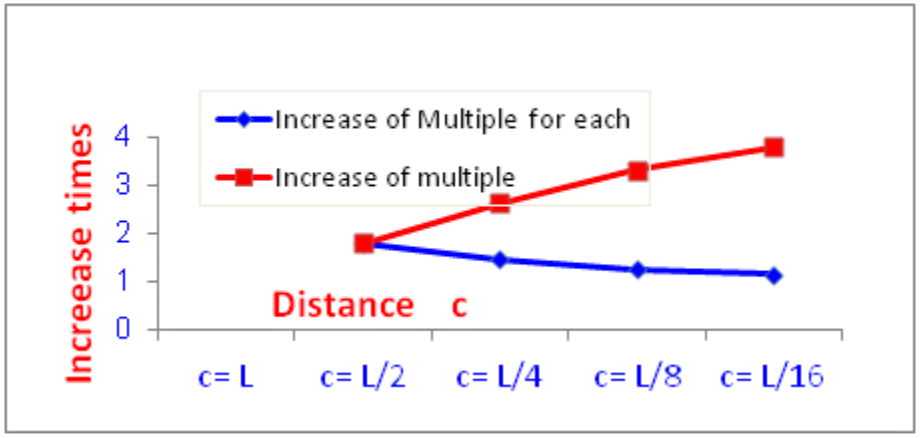

Figure 3.10 Relationship between Side Force and Distance c (when a=ℓ/4, b=3ℓ/4)

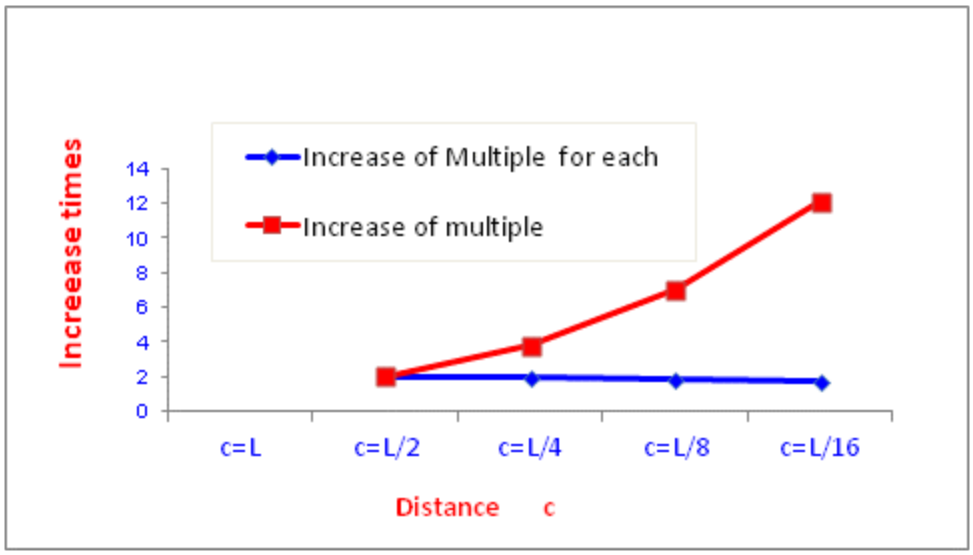

Figure 3.11 Relationship between Side Force and Distance c (when a=b=ℓ/2)

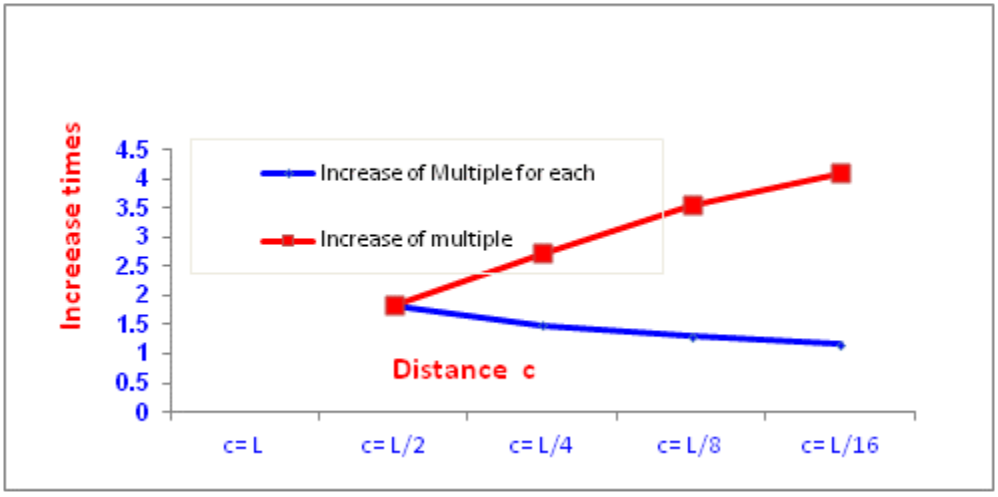

Figure 3.12 Relationship between Side Force and Distance c (when a=3ℓ/4, b=ℓ/4)

3.3 Flexural Distortion Analysis of the Mandrel in an Orienting RSS

3.3.1 Introduction

Orienting RSS technology has been extensively applied in the petroleum industry since the 1990's. This technology can be integrated with the trajectory controlling method and measurement while drilling. It has been successfully applied in deflected wells and multi-lateral wells [21] [22]. Even for exploration wells, this technology can be cost effective.

It is known that the steering drilling tool is much more reliable when building angles than other methods, because its way of building angles does not rely on the formation properties, but rather depends on its design. A biasing apparatus is placed in the center of the steering drilling tool. During the drilling, the steering drilling tool can be deflected when the biasing apparatus pushes the mandrel around in order to build angle and control the trajectory [23] [24].

As we know, the biasing apparatus is placed in the internal cylinder of a steering drilling tool. The bended mandrel is deviated from the axial line to control the wellbore trajectory, to adjust the variance of curvature, and to change the building angle. Since the formation properties have no effect on its angle building, the orienting rotary steerable drilling tool is quite stable and reliable.

Some experimental and theoretical studies have been conducted to better design the steerable drilling tools [30]. However, no studies related to flexural distortion of the mandrel and selection of supporting points has been found in the literature. The mechanical and mathematical models have been built to understand the relationship

between the flexural distortion curve and the axial length (λ) of a mandrel. These investigations and analysis provide a more effective way to design the orienting rotary steerable drilling tools.

3.3.2 Mechanical model

An orienting RSS comprises six major components; drilling bit, lower bearing, biasing apparatus, mandrel, upper bearing, and cylinder, as shown in the Figure 3.13.

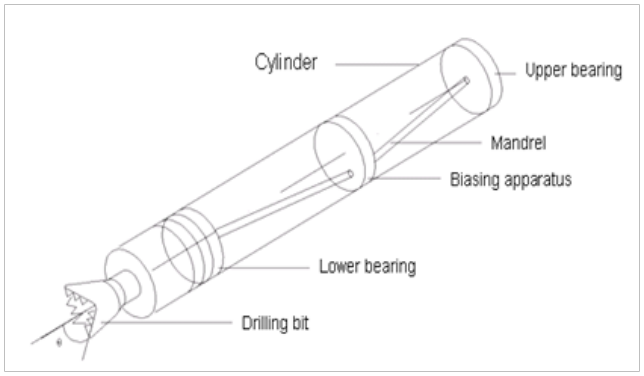

Figure 3.13 Schematic Diagram of Orienting Rotary Steerable Drilling Tool

The principle is the drilling bit deviates from the axial line of the wellbore at a draft angle θ when the biasing apparatus bends the mandrel, in order to control the wellbore trajectory, to increase/decrease wellbore angle, and to adjust the orientation of the wellbore.

The coordinate system is built in accordance with the axial line of the orienting RSS. It is assumed that:

The lower bearing is a hinge joint; The upper bearing is a sliding hinge joint; The load is concentrated at one point of a mandrel, referred as P; The mass of the mandrel is quite small and negligible; There is no drilling load along the axial direction of the mandrel due to its particular design.

Based on the assumptions above, the mechanical model of a mandrel is indicated as Figure 3.14.

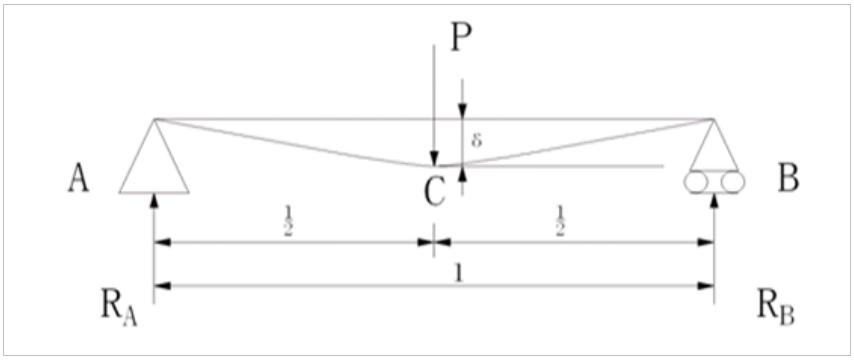

Figure 3.14 Mechanic Model of the Mandrel in Orienting RSS

Based on the assumptions above, the mechanical model of a mandrel is indicated as Figure 3.14.

In respect of the above mechanic model, the differential equations of the mandrel are as follows [25]:

When 0<x<c, M1=RA*x

$$\therefore EJy_1'' = M_1 = \frac{P}{2}x \tag{3.81}$$

$$EJy_1' = \frac{Px^2}{4} + C_1 \tag{3.82}$$

$$EJy_1 = \frac{Px^3}{12} + C_1 x + D_1 \tag{3.83}$$

When $\frac{l}{2} \le x \le l$, $M_2 = \frac{Px}{2} - P(x - \frac{l}{2})$

$$\therefore EJy_2'' = M_2 = \frac{P}{2}x - P(x - \frac{l}{2}) \tag{3.84}$$

$$EJy_2' = \frac{Px^2}{4} - P(\frac{x^2}{2} - \frac{l}{2}x) + C_2 \tag{3.85}$$

$$EJy_2 = \frac{Px^3}{12} - P(\frac{x^3}{6} - \frac{lx^2}{4}) + C_2 x + D_2 \tag{3.86}$$

Applying boundary condition ($x = 0$, y_1=0) to Equation (3.83), $D_1 = 0$ (3.87)

Applying $x = \frac{l}{2}$, $y_1' = 0$ to Equation (3.82):

$$C_1 = -\frac{Pl^2}{16} \tag{3.88}$$

Applying $x = l$, $y_2 = 0$ to Equation (3.86):

$$D = \frac{Pl^3}{6} + C_2 l + D_2 \tag{3.89}$$

Applying $x = \frac{l}{2}$, $y_2' = 0$ to Equation (3.85):

$$D = \frac{3Pl^2}{16} + C_2 \tag{3.90}$$

Combined Equations (3.89) and (3.90), $C_2 = -\frac{3Pl^2}{16}$ (3.91)

$$D_2 = \frac{Pl^3}{48} \tag{3.92}$$

When $0< x \leq \frac{l}{2}$:

The rotating and deflection equations are obtained by applying Equations (3.87) and (3.88) into equations (3.82) and (3.83):

$$\theta = \frac{P}{16EJ}(4x^2 - l^2) \tag{3.93}$$

$$y = \frac{P}{48EJ}(4x^3 - 3l^2) \tag{3.94}$$

When $\frac{l}{2} \leq x \leq l$:

The rotor angle and flexivity equations are obtained by applying Equations (3.91) and (3.92) into Equations (3.85) and (3.86):

$$\theta = \frac{P}{16EJ}(8lx - 4x^2 - 3l^2) \tag{3.95}$$

$$y = \frac{P}{48EJ}(l^3 - 9l^2x + 12lx^2 - 4x^3) \tag{3.96}$$

In equations (3.83) and (3.86)， when $x = \frac{l}{2}$:

The max flexivity is obtained:

$$y_{\max} = -\frac{Pl^3}{48EJ} \tag{3.97}$$

Meanwhile, when beam is bended, the expression of axial offsetting is [26]:

$$\lambda = \frac{1}{2}\int_0^l (\frac{dy}{dx})^2 dx \tag{3.98}$$

Differentiating Equation (3.94):

$$y' = \frac{Px^2}{48EJ} - \frac{Pl^2}{16EJ} \tag{3.99}$$

Applying Equation (3.99) to (3.96), then:

$$\lambda = \frac{1}{2}\int_0^l (\frac{Px^2}{4EJ} - \frac{Pl^2}{16EJ})^2 dx$$

And, it is obtained that $\lambda = \frac{23P^2l^5}{7680E^2J^2}$ (3.100)

The force H for elongated beam is [27]:

$$H = \frac{EA\lambda}{l} \tag{3.101}$$

Applying Equation (3.100) to (3.101), then

$$H = \frac{23P^2l^4A}{7680J^2} \tag{3.102}$$

And, the tension stress σ is:

$$\sigma = \frac{H}{A} \tag{3.103}$$

Applying Equation (3.102) to (3.103), then

$$\sigma = \frac{23P^2l^4}{7680EJ^2} \tag{3.104}$$

3.3.3 Discussion

With the establishment of the mandrel mechanical model and the flexivity equation, the flexivity of a mandrel and axial offsetting have been determined for a distortional mandrel. That is, for a specific design of orienting rotary steerable drilling tool, the constraint conditions have been decided. The retracted distance can thus be solved for a bended mandrel.

As shown in Equation (3.84), the flexivity of mandrel is proportional to the single point load and is inversely proportional to anti-bend modulus. That is the higher single point load, the larger flexivity and the larger anti-bend modulus, the smaller flexivity. As shown as Equation (3.97), the flexivity is the largest at the middle point of mandrel. Inversely, given a specific flexivity, the single point load is as followed.

$$P = -\frac{48EJy_{\max}}{l^3} \tag{3.105}$$

Equation (3.105) is quite useful in designing the drilling tool to understand the single point load since the maximum flexivity is predetermined. It is also shown that single point load is inversely proportional to l_3. The increase of mandrel length reduces the single point load. However, the mandrel length is normally restrained by the size of tools. As shown in Equation (3.104), the tension stress is proportional to P_2 and is inversely proportional to l4 and EJ. In order to reduce the tension stress, the material with a higher elastic modulus E and a larger cross section should be chosen.

3.3.4 Case studies

An example is given to demonstrate the design of an orientating rotary steerable drilling tool assuming a 6¾" (Φ171.45mm) drilling collar and a orientating rotary steerable drilling tool applied in a 8½" (Φ215.9mm) wellbore, Mandrel length (l=400cm), outer diameter (OD=95cm), and inner diameter (ID=45cm). Biasing apparatus is placed in the middle of drilling tool (AC=200cm) with a maximum flexivity (y_{max}=2cm).

With reference to Equation (3.105), the single point load P is

$$P = \frac{48 \times 2.1 \times 10^6 \times 379.5 \times 2}{400^3} = 1195.4kg$$

With reference to Equation (3.100), the axial offsetting of mandrel is

$$\lambda = \frac{23 \times 1195.4^2 \times 400^2}{7680 \times (2.1 \times 10^6 \times 379.5)^2} = 0.069cm$$

With reference to Equation (3.104), when the two ends of bended mandrel are fixed the tension stress is

$$\sigma = \frac{23 \times 1195.4^2 \times 400^4}{7680 \times 2.1 \times 10^6 \times 379.5^2} = 0.995kg/cm^2$$

Using the same method, a datasheet, as shown in Table 3.6, has been made to show the calculation results of the single point load, tension stress and axial offsetting under different tool size.

Table 3.6 shows that when the geometric size of mandrel is determined, i.e., inner and outer diameter, material, and elastic modulus, the mechanical properties of this mandrel is:

When mandrel length is determined, with the increase of flexivity y, single point load P, axial offsetting λ and tension stress σ are increased. As shown from No. 1 to No. 4 of Table 3.6, when flexivity y increases from 1cm to 4cm, P, λ, and σ increase from 1416.8kg to 5667.2kg, 0.023cm to 0.336cm, 0.42kg/cm^2 to 6.788kg/cm^2, respectively.

When flexivity y is determined, with the increase of mandrel length l, single point load P, axial offsetting λ and tension stress σ are decreased. For example, as shown in No. 4, 8, 12, and 16 of Table 3.6, when mandrel length l increase, P, λ, and σ decrease from 5666.7kg to 708.4kg, 0.368cm to 0.184cm, 6.788kg/cm^2 to 1.697kg/cm^2, respectively. The analysis as shown in Table 3.6 can be used to guide the design of orienting rotary steerable drilling tools.

3.3.5 Conclusions

Mandrel design is better understood based on our study and analysis of the orienting RSS. As normally when designing a mandrel, it is assured that no drilling load is applied along the axial direction. Thus, the proposed model in this paper can be used to calculate the flexural distortion of mandrels.

Flexivity of a mandrel is determined by a specific biasing apparatus. Meanwhile, the single point load can be solved with a given flexivity. It's quite helpful to design the mandrel for the RSS.

In order to avoid the drilling load being applied along the axial direction of a mandrel, one of the supporting points of the mandrel must be a sliding hinge joint. It is necessary to leave an axial offset in advance for the mandrel. Thus, the methodology

proposed in this paper to calculate the axial offsetting of the mandrel is important and meaningful.

The distortion and the load on a mandrel can be easily calculated by using the proposed model. The tension stress and axial offset of a mandrel can be used to understand the intension. It is helpful to better understand the properties and performance of the orienting RSS. The relationship between deflection and bending stress is shown in Table 3.6. The relationship between displacement and bending stress of case 1 is shown in Figure 3.15.

Table 3.6 Relationship between Deflection and Bending Stress

No	OD cm	ID cm	polar moment of inertia J cm^4	elastic modulus E ksc	deflection y cm	L cm	concentrate load P kg	shift λ cm	bending stress σ kg/cm2
1	9.5	4.5	379.69	2100000	1	300	1417.5	0.023	161.0
2	9.5	4.5	379.69	2100000	2	300	2835.0	0.092	644.0
3	9.5	4.5	379.69	2100000	3	300	4252.5	0.207	1449.0
4	9.5	4.5	379.69	2100000	4	300	5670.1	0.368	2576.0
5	9.5	4.5	379.69	2100000	1	400	598.0	0.017	90.6
6	9.5	4.5	379.69	2100000	2	400	1196.0	0.069	362.3
7	9.5	4.5	379.69	2100000	3	400	1794.0	0.155	815.1
8	9.5	4.5	379.69	2100000	4	400	2392.1	0.276	1449.0
9	9.5	4.5	379.69	2100000	1	600	177.2	0.012	40.3
10	9.5	4.5	379.69	2100000	2	600	354.4	0.046	161.0
11	9.5	4.5	379.69	2100000	3	600	531.6	0.104	362.3
12	9.5	4.5	379.69	2100000	4	600	708.8	0.184	644.0
13	9.5	4.5	379.69	2100000	1	800	74.8	0.009	22.6
14	9.5	4.5	379.69	2100000	2	800	149.5	0.035	90.6
15	9.5	4.5	379.69	2100000	3	800	224.3	0.078	203.8
16	9.5	4.5	379.69	2100000	4	800	299.0	0.138	362.3
17	9.5	4.5	379.69	2100000	1	1000	38.3	0.007	14.5
18	9.5	4.5	379.69	2100000	2	1000	76.5	0.028	58.0
19	9.5	4.5	379.69	2100000	3	1000	114.8	0.062	130.4
20	9.5	4.5	379.69	2100000	4	1000	153.1	0.110	231.8

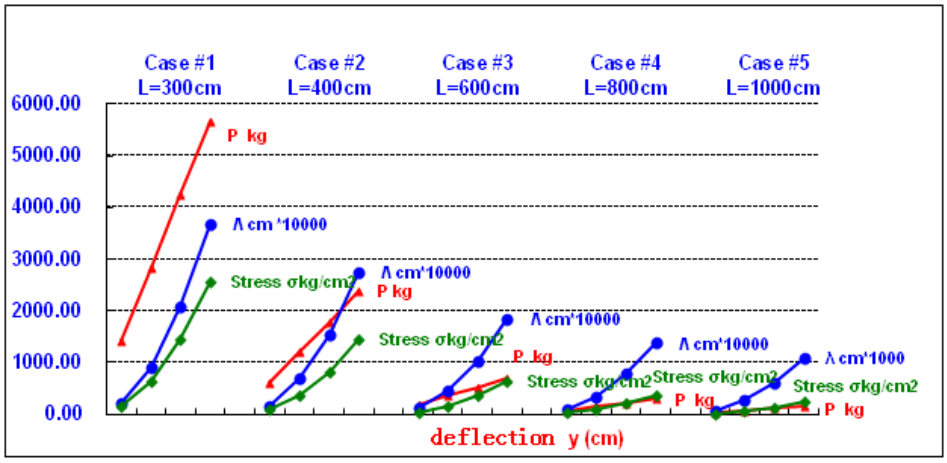

Figure 3.15 Relationship between Deflection and Bending Stress of Case 1

3.4 Research on the Mechanical Properties and Design Methods of Point-the-bit Rotary Steerable Drilling Tools

The RSS is widely used in offshore and onshore drilling operations. In particular, it has played an important role in offshore cluster wells and directional drilling work. Rotary steerable drilling technology has high trajectory controlled precision. Directional wells can complete the twisted position, orientation and other operations, improving the cleanliness of the borehole, which greatly reduces the risk of stuck pipe. RSS technology is becoming an important development trend in drilling.

Among the present RSS, the point-the-bit RSS by Halliburton Company in the United States is preferred by engineers. This is because the slope of the mandrel is determined by making the biasing force through biasing the bend. These result in the manufacture of the oblique in which formation of the force is negligible, thereby making the slope more stable.

However, how can we give the tools a better build up ability to improve the stability of its work, as well as making a more rationally designed tool? This requires in depth study and exploration.

3.4.1 Issues raised

Point-the-bit RSS in directional wells operation is characterized by a relatively high build rate, especially in shallow soft formations whipstock has obvious advantages. But after entering the deep strata, what engineers expect more is a longer tool life. Therefore, first we should start with the structure of the tools to analyze and understand the mechanical properties.

RSS structure is shown in Figure 3.16. A: Tool mandrel upper bearing, B: Tool mandrel lower bearing, C: Bit, D: Offset wheels, as well as housing and mandrel.

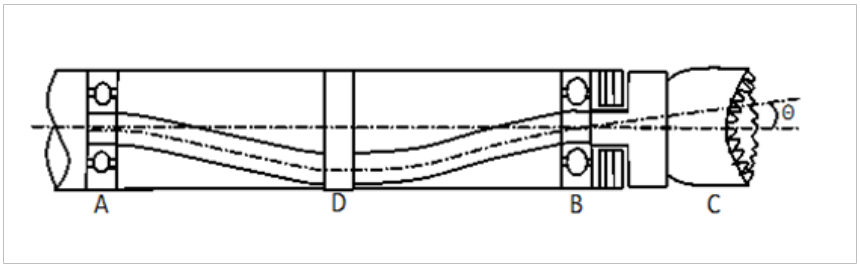

Figure 3.16 Point-the-Bit Rotary Steerable Drilling Tool Schematic Structure

The main working principle is the effect on the bias roller D under the concentrated load P on the mandrel, producing the mandrel bend. The lateral force

generated at the drill bit and the corner makes the tools deflect. This bending mandrel is caused when the bias wheel and the tool steel casing come in contact.

Because the bending mandrel is generated by the contact between the bias wheel and the tool housing, the ability of the tool's whipstocking does not depend on the hardness of the ground, but only with the control of the tool itself. So the tool has enhanced buildup rate.

3.4.2 Point-the-bit rotary steerable drilling tool mandrel mechanics model

To make the study of the problem simple and convenient, we first make the following assumptions:

(1) Take the tool mandrel upper bearing A and lower bearing B as hinge pivot, meanwhile, take the bit as solid fulcrum.

(2) Take the biasing force on the bias wheel as concentrated force P, it causes mandrel bending.

(3) The quality of the mandrel is a continuous distribution, and its weight per unit length is q, its load and the axis orthogonal is the vertical distribution, the load is uniform load $q\sin\alpha$.

(4) The mandrel can be regarded as not subjected to axial force because WOB is applied only on the casing.

(5) Alone the axial direction of the drill and the mandrel, in order to establish the coordinate system, the direction of the X axis is positive, so that we can get the mechanical model (case 1) shown in Figure 3.17.

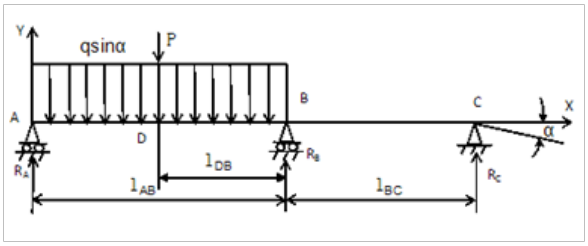

Figure 3.17 Mechanical Model of Mandrel (Case 1)

The mechanical model of the mandrel is: the bearing A, B and the bit C subjected to reaction forces R_A, R_B and R_C, the mandrel subjected to uniform load qsinα and biasing force P. So we solve the problem of the bit side force R_C by treating this model as uncertain beam problem.

When $\ell_{AB}=\ell_{BC}$, we can get the mechanical model (case 2) shown in Figure 3.18.

This is a statically indeterminate problem; R_A is a redundant reaction force, according to the static equilibrium conditions α obtained:

$$\sum M_C = 0$$

$$R_B l = -2R_A l + \frac{3Pl}{2} + \frac{3ql^2 \sin\alpha}{2} = -2R_A l + \frac{3l}{2}\left(P + ql\sin\alpha\right)$$

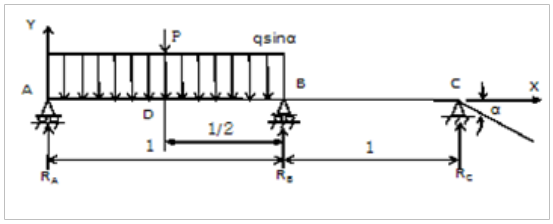

Figure 3.18 Mechanical Model of Mandrel (Case 2)

$$R_B = -2R_A + \frac{3}{2}\left(P + ql\sin\alpha\right) \tag{3.106}$$

$$\sum M_B = 0$$

$$R_C l = R_A l - \frac{Pl}{2} - \frac{ql^2\sin\alpha}{2} = R_A l - \frac{l}{2}\left(P + ql\sin\alpha\right)$$

$$R_C = R_A - \frac{1}{2}\left(P + ql\sin\alpha\right) = R_A - \frac{1}{2}\left(P + ql\sin\alpha\right) \tag{3.107}$$

Each point bending of beam:

Section AD: $$M_1 = R_A x - \frac{qx^2\sin\alpha}{2} \tag{3.108}$$

Section AB: $$M_2 = R_A x - P(x - \frac{l}{2}) - \frac{qx^2\sin\alpha}{2} \tag{3.109}$$

Section AC: $$M_3 = R_A x + R_B(x-l) - P(x-\frac{l}{2}) - ql(x-\frac{l}{2})\sin\alpha \tag{3.110}$$

$$M_3 = R_A x + \left[-2R_A + \frac{3}{2}(P + ql\sin\alpha)\right](x-l) - P(x-\frac{l}{2}) - ql(x-\frac{l}{2})\sin\alpha$$

$$= R_A\left[-2R_A x + 2R_A l + \frac{3}{2}Px - \frac{3}{2}Pl + \frac{3ql\chi}{2}\sin\alpha - \frac{3ql^2\sin\alpha}{2}\right] - Px + \frac{Pl}{2} - qlx\sin\alpha + \frac{ql^2}{2}\sin\alpha$$

$$= 2R_A l - R_A x + \frac{Px}{2} - Pl + \frac{ql}{2}x\sin\alpha - ql^2\sin\alpha$$

$$= R_A(2l-x) + P(\frac{x}{2} - l) + ql(\frac{x}{2} - l)\sin\alpha = -R_A(x-2l) + \frac{P}{2}(x-2l) + \frac{ql}{2}(x-2l)\sin\alpha$$

$$M_3 = R_A(2l-x) + (P + ql\sin\alpha)(\frac{x}{2} - l) \tag{3.111}$$

Then the strain complementary energy of beam [28] [29]:

$$U = \frac{1}{2EJ}\int_0^{\frac{l}{2}}\left(R_A x - \frac{qx^2\sin\alpha}{2}\right)^2 d_x + \int_{\frac{l}{2}}^{l}\left[R_A x - P\left(x - \frac{l}{2}\right) - \frac{qx^2\sin\alpha}{2}\right]^2 d_x + \int_l^{2l}\left[(x-2l)\left(-R_A + \frac{P}{2} + \frac{ql}{2}\sin\alpha\right)\right]^2 d\ x \tag{3.112}$$

Application of minimum complementary energy principle can be obtained:

$$\frac{\partial \pi}{\partial R_A}=\frac{1}{2EJ}\left\{\int_0^{\frac{l}{2}}\left(R_A x-\frac{qx^2\sin\alpha}{2}\right)d_x+\int_{\frac{l}{2}}^{l}2x\left[R_A x-P\left(x-\frac{l}{2}\right)-\frac{qx^2\sin\alpha}{2}\right]d_x+\int_l^{3l}\left[-2\left(-R_A+\frac{P}{2}+\frac{ql}{2}\sin\alpha\right)(x-2l)^2\right]d_x\right\} \quad (3.113)$$

Integrate:

$$R_A=\frac{13}{32}P+\frac{1}{16}ql\sin\alpha=0.41P+0.125ql\sin\alpha \quad (3.114)$$

Substituting (3.114) into (3.106) can be obtained:

$$R_B=\frac{37}{16}P+\frac{7ql\sin\alpha}{4}=2.31P+1.75ql\sin\alpha \quad (3.115)$$

Substituting (3.114) into (3.107) can be obtained:

$$R_C=-\frac{3P}{32}-\frac{3ql\sin\alpha}{8}=-\left(0.09P+0.375ql\sin\alpha\right) \quad (3.116)$$

When $\ell_{AB}=2\ell_{BC}$, we can get the mechanical model (case 3) shown in Figure 3.19.

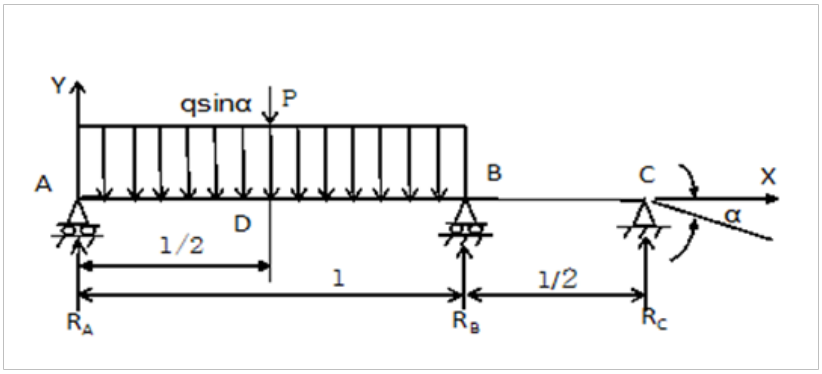

Figure 3.19 Mechanical Model of Mandrel (Case 3)

$$\sum M_c = 0$$

$$\frac{R_B l}{2} = -\frac{3R_A l}{2} + Pl + ql^2 \sin\alpha$$

$$R_B = -3R_A + 2P + 2ql\sin\alpha \tag{3.117}$$

$$\sum M_B = 0$$

$$\frac{R_C l}{2} = R_A l - \frac{Pl}{2} - \frac{ql^2}{2}\sin\alpha$$

$$R_C = 2R_A - P - ql\sin\alpha \tag{3.118}$$

Each point bending of beam:

Section AD:
$$M_1 = R_A x - \frac{qx^2\sin\alpha}{2} \tag{3.119}$$

Section AB:
$$M_2 = R_A x - P(x - \frac{l}{2}) - \frac{qx^2\sin\alpha}{2} \tag{3.120}$$

Section AC:
$$M_3 = R_A x + R_B(x-l) - P(x-\frac{l}{2}) - ql(x-\frac{l}{2})\sin\alpha \tag{3.121}$$

$$M_3 = R_A X + (-3R_A + 2P + 2ql\sin\alpha)(X-l) - PX + \frac{Pl}{2} - qlX + \frac{ql^2\sin\alpha}{2}$$

$$= R_A X + (-3R_A X + 3R_A l + 2PX - 2Pl + 2qlX\sin\alpha - 2ql^2\sin\alpha) - PX + \frac{Pl}{2} - qlX + \frac{ql^2}{2}\sin\alpha$$

$$= 3R_A l - 2R_A X + PX - \frac{3Pl}{2} + qlX\sin\alpha - \frac{3ql^2}{2}\sin\alpha$$

$$= R_A(3l - 2X) + \frac{P}{2}(2X - 3l) + \frac{ql}{2}(2X - 3l)\sin\alpha$$

$$M_3 = R_A(2l - x) + (P + ql\sin\alpha)(\frac{x}{2} - l) \tag{3.122}$$

Then the strain complementary energy of beam:

$$U=\frac{1}{2EI}\left\{\int_0^{\frac{l}{2}}\left(R_A X-\frac{ql^2}{2}\right)^2 dX+\int_{\frac{l}{2}}^{l}\left[R_A X-\frac{P}{2}\left(X-\frac{l}{2}\right)-\frac{qX^2}{2}\right]^2 dX+\int_l^{3l/2}\left(-R_A+\frac{P}{2}+\frac{ql}{2}\right)^2 dX\right\} \quad (3.123)$$

Application of minimum complementary energy principle can be obtained:

$$\frac{\partial\pi}{\partial R_A}=\frac{1}{2EJ}\{\int_0^{\frac{l}{2}}2\left(R_A X-\frac{qX^2\sin\alpha}{2}\right)^2 XdX+\int_{\frac{l}{2}}^{l}2\left[R_A X-P\left(X-\frac{l}{2}\right)-\frac{qX^2\sin\alpha}{2}\right]^2 XdX+$$
$$\int_l^{3l/2}\left[R_A(2l-x)+(\frac{x}{2}-l)(P+ql\sin\alpha)\right]^2 dX\} \quad (3.124)$$

Integrate:

$$R_A=\frac{2}{5}P+\frac{13}{30}ql\sin\alpha=0.4P+0.43ql\sin\alpha \quad (3.125)$$

$$R_B=\frac{4}{5}P+\frac{7}{10}ql\sin\alpha=0.8P+0.7ql\sin\alpha \quad (3.126)$$

$$R_C=-\left(\frac{P}{5}+\frac{2}{15}ql\sin\alpha\right)=-(0.2P+0.13ql\sin\alpha) \quad (3.127)$$

When $\ell_{AB}=2\ell_{BC}=4\ell_{BD}$, we can get the mechanical model (case 4) shown in Figure 3.20.

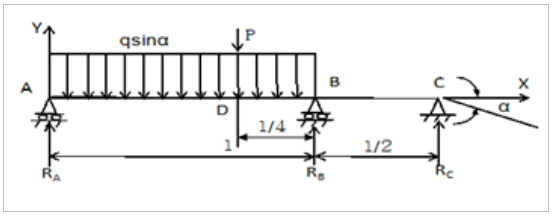

Figure 3.20 Mechanical Model of Mandrel (Case 4)

$$\Sigma M_C = 0$$

$$\frac{R_B l}{2} + \frac{3}{2} R_A l = \frac{3}{4} Pl + ql^2 \sin\alpha$$

$$R_B = -3 R_A + \frac{3P}{2} + 2ql\sin\alpha \tag{3.128}$$

$$\Sigma M_B = 0$$

$$\frac{R_C l}{2} + \frac{Pl}{4} + \frac{ql^2}{2}\sin\alpha = R_A l$$

$$\frac{R_C}{2} + \frac{P}{4} + \frac{ql}{2}\sin\alpha = R_A$$

$$R_C = 2 R_A - \frac{P}{2} - ql\sin\alpha \tag{3.129}$$

Each point bending of beam:

Section AD:
$$M_1 = R_A X - \frac{qX^2 \sin\alpha}{2} \tag{3.130}$$

Section AB:
$$M_2 = R_A X - p\left(X - \frac{3l}{4}\right) - \frac{qX^2 \sin\alpha}{2} \tag{3.131}$$

Section AC:
$$M_3 = R_A X + R_B (X - l) - P\left(X - \frac{3}{4}l\right) - ql\left(X - \frac{l}{2}\right)\sin\alpha \tag{3.132}$$

Substituting (3.128) into (3.132) can be obtained:

$$M_3 = R_A X + \left(\frac{3}{2}P + 2ql - 3R_A\right)(X - l) - PX + \frac{3}{4}Pl - qlX + \frac{ql^2}{2}$$

$$M_3 = R_A X + \frac{3}{2}PX - \frac{3}{2}Pl + 2qlX\sin\alpha - 2ql^2 - 3R_A X + 3R_A l - PX + \frac{3}{4}Pl - qlX\sin\alpha + \frac{ql^2}{2}\sin\alpha$$
$$= 3R_A l - 2R_A X + \frac{PX}{2} - \frac{3}{4}Pl + qlX\sin\alpha - \frac{3}{2}ql^2\sin\alpha$$

$$= R_A(3l-2X)-P\left(\frac{3l}{4}-\frac{X}{2}\right)-ql\left(\frac{3}{2}l-X\right)\sin\alpha$$

$$M_3 = R_A(3l-2X)-\frac{P}{4}(3l-2X)-\frac{ql}{2}(3l-2X)\sin\alpha \tag{3.133}$$

Then the strain complementary energy of beam:

$$U=\frac{1}{2EJ}\int_0^{\frac{3l}{4}}\left(R_A X-\frac{qX^2}{2}\sin\alpha\right)^2 dX+\int_{\frac{3l}{4}}^{l}\left[R_A X-P\left(X-\frac{3l}{4}\right)-\frac{qX^2\sin\alpha}{2}\right]^2 dX$$

$$+\int_l^{3l/2}\left[(3l-2X)\left(R_A-\frac{P}{4}-\frac{ql\sin\alpha}{2}\right)\right]^2 dX \tag{3.134}$$

Application of minimum complementary energy principle can be obtained:

$$\frac{\partial\pi}{\partial R_A}=\frac{1}{2EJ}\int_0^{\frac{3l}{4}}2\left(R_A X-\frac{ql^2}{2}\sin\alpha\right)XdX+\int_{\frac{3l}{4}}^{l}2\left[R_A X-P\left(X-\frac{3l}{4}\right)-\frac{qX^2\sin\alpha}{2}\right]XdX$$

$$+\int_l^{3l/2}\left[2(3l-2X)^2\left(R_A-\frac{P}{4}-\frac{ql\sin\alpha}{2}\right)\right]dX \tag{3.135}$$

Integrate:

$$R_A=\frac{9}{64}P+\frac{5}{12}ql\sin\alpha=0.14P+0.416ql\sin\alpha \tag{3.136}$$

$$R_B=\frac{69}{64}P+\frac{3}{4}ql\sin\alpha=1.07P+0.75ql\sin\alpha \tag{3.137}$$

$$R_C=-\frac{7}{32}P-\frac{1}{6}ql\sin\alpha=-0.21P-0.166ql\sin\alpha \tag{3.138}$$

When $\ell_{AB}=\frac{4\ell_{AD}}{3}=10\ell_{BC}$, we can get the mechanical model (case 5) shown in Figure 3.21.

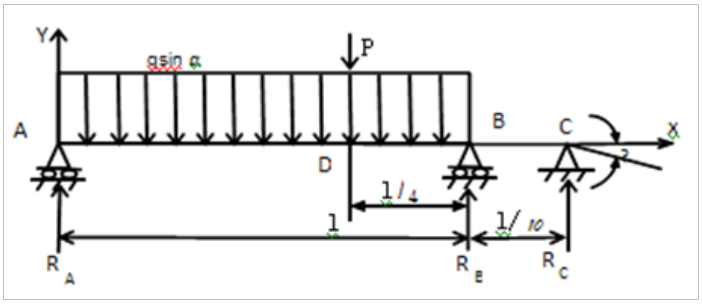

Figure 3.21 Mechanical Model of Mandrel (Case 5)

Similarly: $\sum M_c = 0$

$$R_A \frac{11l}{10} + \frac{R_B l}{10} = \frac{7pl}{20} + \frac{6ql^2}{10}\sin\alpha \qquad 11R_A l + R_B \ell = \frac{7}{2}pl + 6ql^2\sin\alpha$$

$$R_B = \frac{7}{2}p + 6ql\sin\alpha - 11R_A \tag{3.139}$$

$\sum M_B = 0$

$$R_A l = \frac{R_C l}{10} + \frac{pl}{4} + \frac{ql^2}{2}\sin\alpha \qquad 10R_A = R_C + \frac{5p}{2} + 5ql\sin\alpha$$

$$R_c = 10R_A - \frac{5p}{2} - 5ql\sin\alpha \tag{3.140}$$

Each point bending of beam:

Section AD：
$$M_1 = R_A x - \frac{qx^2\sin\alpha}{2} \tag{3.141}$$

Section AB：
$$M_2 = R_A x - p\left(x - \frac{3}{4}l\right) - \frac{ql^2}{2}\sin\alpha \tag{3.142}$$

Section AC:

$$M_3 = R_A x + R_B(x-l) - p\left(x-\frac{3l}{4}\right) - ql\left(x-\frac{l}{2}\right) \tag{3.143}$$

Substituting (3.139) into (3.143) can be obtained:

$$M_3 = R_A x + \left(\frac{7}{2}p + 6ql - 11R_A\right)(x-l) - p\left(x-\frac{3l}{4}\right) - ql\left(x-\frac{l}{2}\right)$$

$$M_3 = R_A x + \frac{7}{2}px - \frac{7pl}{2} + 6qlx\sin\alpha - 6ql^2\sin\alpha - 11R_A x + 11R_A l - px + \frac{3pl}{4} - qpx\sin\alpha + \frac{ql^2}{2}\sin\alpha$$

$$= 11R_A l - 10R_A x + \frac{5}{2}px - \frac{11pl}{4} + 5pqx\sin\alpha - \frac{11}{2}ql^2\sin\alpha$$

$$= R_A(11l-10x) + \frac{p}{4}(10x-11l) + \frac{ql}{2}(10x-11l)\sin\alpha$$

$$M_3 = (10x-11l)\left(-R_A + \frac{p}{4} + \frac{ql}{2}\sin\alpha\right) \tag{3.144}$$

Then the strain complementary energy of beam:

$$U = \frac{1}{2EJ}\left[\int_0^{\frac{3l}{4}}\left(R_A x - \frac{qx^2}{2}\sin\alpha\right)^2 dx + \int_{\frac{3l}{4}}^{l}\left[R_A x - p\left(x-\frac{3l}{4}\right) - \frac{ql^2\sin\alpha}{2}\right]^2 dx + \int_l^{\frac{11l}{10}}\left[(10x-11l)\left(-R_A + \frac{P}{4} + \frac{ql\sin\alpha}{2}\right)\right]^2 dx\right] \tag{3.145}$$

Application of minimum complementary energy principle can be obtained:

$$\frac{\partial\pi}{\partial R_A} = \frac{1}{2EJ}\left[\int_0^{\frac{3l}{4}} 2\left(R_A x - \frac{qx^2}{2}\sin\alpha\right)dx + \int_{\frac{3l}{4}}^{l} 2\left[R_A x - p\left(x-\frac{3l}{4}\right) - \frac{ql^2\sin\alpha}{2}\right]x\,dx + \int_l^{\frac{11l}{10}} -2(11l-10x)^2\left(-R_A + \frac{p}{4} + \frac{ql}{2}\sin\alpha\right)dx\right] \tag{3.146}$$

Integrate:

$$R_A = \frac{71}{704}P + \frac{5087ql}{11264}\sin\alpha \qquad R_A = 0.1P + 0.45ql\sin\alpha \tag{3.147}$$

$$R_B = \frac{153}{64}P + \frac{1057}{1024}ql\sin\alpha \qquad R_B = 2.3p + 1.03ql\sin\alpha \tag{3.148}$$

$$R_C = -\left(\frac{525}{352}p + \frac{2725}{5632}ql\sin\alpha\right) \quad R_C = -\left(1.49p + 0.48ql\sin\alpha\right) \tag{3.149}$$

When $\ell_{AB}=4\ \ell_{AD}=10\ \ell_{BC}$, we can get the mechanical model (case 6) shown in Figure 3.22.

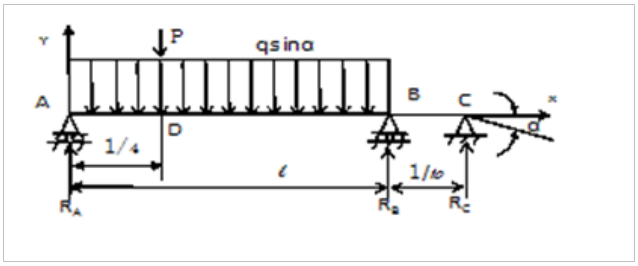

Figure 3.22 Mechanical Model of Mandrel (Case 6)

$$\sum M_C = 0 \quad \frac{11R_A l}{10} + \frac{R_B l}{10} = \frac{17pl}{20} + \frac{6ql^2}{10}\sin\alpha$$

$$R_B = \frac{17p}{2} + 6ql^2\sin\alpha - 11R_A \tag{3.150}$$

$$\sum M_B = 0$$

$$R_A l = \frac{R_C l}{10} + \frac{3pl}{4} + \frac{ql^2\sin\alpha}{2} \qquad R_C = 10R_A - \frac{15p}{2} - 5ql\sin\alpha \tag{3.151}$$

Each point bending of beam:

Section AD: $$M_1 = R_A x - \frac{qx^2\sin\alpha}{2} \tag{3.152}$$

Section AB: $$M_2 = R_A x - p\left(x - \frac{l}{4}\right) - \frac{qx^2\sin\alpha}{2} \tag{3.153}$$

Section AC: $$M_3 = R_A x + R_B(x-l) - p\left(x-\frac{l}{4}\right) - ql\left(x-\frac{l}{2}\right)\sin\alpha \qquad (3.154)$$

Substituting (3.150) into (3.154) can be obtained:

$$M_3 = R_A x + \left(\frac{17}{2}P + 6ql^2\sin\alpha - 11R_A\right)(x-l) - px + \frac{pl}{4} - qlx + \frac{ql^2\sin\alpha}{2}$$

$$\mathrm{M_3} = R_A x + \frac{17}{2}px + \frac{17}{2}pl + 6ql^2x - 6ql^2\sin\alpha - 11R_A x + 11R_A l$$

$$- px - \frac{pl}{4} - qlx + \frac{ql^2}{2}\sin\alpha$$

$$M_3 = R_A(11l-10x) + \frac{33p\ell}{4} - \frac{15px}{2} + 5qlx\sin\alpha - \frac{11ql^2\sin\alpha}{2}$$

$$= R_A(11l-10x) + \frac{3p}{4}(11l-10x) - \frac{ql}{2}(11l-10x)\sin\alpha$$

$$M_3 = R_A(11l-10x) + \frac{P(30x-33l)}{4} + \frac{1}{2}ql\sin\alpha(10x-11l) \qquad (3.155)$$

Then the strain complementary energy of beam:

$$U = \frac{1}{2EJ}\int_0^{\frac{l}{4}}\left(R_A x - \frac{qx^2}{2}\sin\alpha\right)d_x + \int_{\frac{l}{4}}^{l}\left[R_A x - P\left(x-\frac{l}{4}\right) - \frac{qx^2}{2}\sin\alpha\right]^2 d_x + \int_l^{\frac{11}{10}l}\left[(11l-10x)\left(R_A + \frac{3P}{4} - \frac{ql}{2}\sin\alpha\right)\right]^2 d_x \quad (3.156)$$

Application of minimum complementary energy principle can be obtained:

$$\frac{\partial\pi}{\partial R_A} = \frac{1}{2EJ}\left\{\int_0^{\frac{l}{4}}2\left(R_A x - \frac{qx^2}{2}\sin\alpha\right)xd_x + \int_{\frac{l}{4}}^{l}2\left[R_A x - P\left(x-\frac{l}{4}\right) - \frac{qx^2\sin\alpha}{2}\right]xd_x + \int_l^{\frac{11}{10}l}2(11l-10x)^2\left(R_A + \frac{3}{4}P - \frac{ql\sin\alpha}{2}\right)d\ x\right\}$$

(3.157)

Integrate:

$$R_A = \frac{3}{704}P + \frac{17}{44}ql \ = 0.004\mathrm{P} + 0.38\mathrm{q}\ell\sin\alpha \qquad (3.158)$$

$$R_B = \frac{541}{64}P + \frac{7}{4}ql = 8.54\text{P}+1.75\text{q}\ell\sin\alpha \quad (3.159)$$

$$R_C = \frac{2625}{352}P - \frac{25ql\sin\alpha}{22} = -(7.45\text{P}+1.13\text{q}\ell\sin\alpha) \quad (3.160)$$

3.4.3 Analysis and understanding

The results of the above calculation and solution to bring together, we can get the dynamic model (in different condition) shown in Table 3.7.

Table 3.7 Dynamic Model in Different Condition

No.	Dynamic Model	Length
1	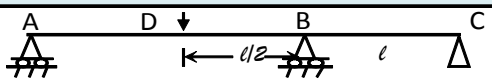	$l_{AB} = l_{BC}$ $l_{AD} = l_{DB} = \frac{l_{AB}}{2}$
2	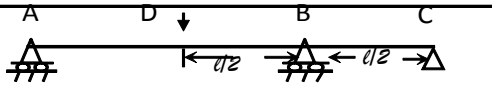	$l_{AB} = 2l_{Bc}$ $l_{AD} = l_{DB} = \frac{l_{AB}}{2}$
3	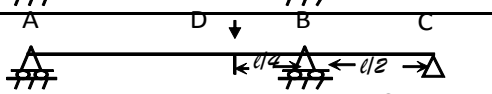	$l_{AB} = 2l_{Bc}$ $l_{AD} = \frac{3}{4}l_{AB}$
4	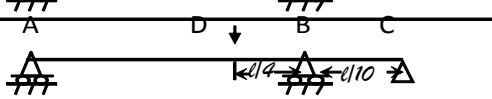	$l_{AB} = 10l_{Bc}$ $l_{AD} = \frac{3}{4}l_{AB}$
5	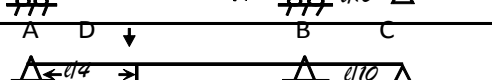	$l_{AB} = 10l_{Bc}$ $l_{AD} = \frac{l_{AB}}{4}$

From table 3.7, we can get the reaction force shown in Table 3.8.

Table 3.8 Reaction Force in Different Condition

No	R_A	R_B	R_C
1	RA=0.41P+0.175q ℓ sinα	RB=2.31P+1.75q ℓ sinα	Rc=-(2.31P+0.375q ℓ sinα)
2	RA=0.4P+0.43 qℓsinα	RB=0.8 P+0.7 qℓsinα	Rc=-(0.2 P+0.133qℓsinα)
3	RA=0.14P+0.41qℓsinα	RB=1.07P+0.75qℓsinα	Rc=-(0.21P+0.166qℓsinα)
4	RA=0.1 P+0.45qℓsinα	RB=2.3 P+1.03qℓsinα	Rc=-(1.49P+0.48 qℓsinα)
5	RA=0.004P+0.14qℓsinα	RB=8.45P+1.75qℓsinα	Rc=-(7.45P+1.13 qℓsinα)

From Table 3.8 we can see:

(1) When the structure unchanged, the biasing load P is farther from the A, a reaction force is smaller, the number 4 and 5 in Table 3.8 is the smallest. When $\ell_{BC}=\ell_{AB}/10$, with the concentrated force P to A moving, R_A5 have smallest force;

(2) Similarly, when $\ell_{AB}=2\ell_{BC}$, i.e., the number 2 and 3 in Table 3.8, with the concentrated load P to B moving, R_B will increase , R_A will decrease.

(3) When l_{AB} constant, shortened l_{BC}, R_B increase, R_C increase.

When $\ell_{BC}=\ell_{AB}/2$, from Table 3.8 No.1 and No.2, we can see: Rc will increase 1.2 times

When $\ell_{BC}=\ell_{AB}/10$, from Table 3.8 No.3 and No.4, we can see: Rc will increase 6 times.

Thus, increasing the bit side force R_C, should try to shorten the distance ℓ_{BC}, then we can get the maximum lateral force R_C.

When we move the bias load P to direction A, $\ell_{AD}=\ell_{AB}/4$, $\ell_{BC}=\ell_{AB}/10$, from Table 3.8 we can see: Rc will increase 4 times. So if we want to get the bigger Rc, the bias load P should be move to A direction.

In summary, we can get some useful insight for designing point-the-bit rotary steerable drilling tool:

(1) From the point of view that to increase the bit side force, we can shorten the extended length of the mandrel, it can largely increase the lateral force on the drill RC.

(2) If in order to increase the lateral force on the drill, but also by changing the bias force P position. When P move far away from the bit, the bit side force has increased more obvious.

(3) From the formulas Rc =AP+Bql, we can see that, the bit side force has relation to the biasing load P, the weight of the mandrel uniform load q and length l. When the mandrel geometry unchanged, ql is a constant. At the moment, the bit side force has only relation to the biasing load P. From the Table 3.8 we can know, by changing the length of the mandrel extending force P and changing the bias point of the position D, it can significantly increase or decrease the lateral force on the bit.

(4) We can increase the size of P, or change the mandrel overhang distance, changing the location of the point P force and other factors to achieve increase the ability to bit side force.

3.4.4 Conclusions

(1) The minimum complementary energy method can be used to analyze mechanical properties of the point-the-bit RSS, and to take appropriate measures to solve the bit side force and buildup ability issues;

(2) There is a significant correlation between design parameters and the buildup ability of point-the-bit rotary steerable drilling tool. Normally, when the bit is farther away from the biasing force, the bit side force will be stronger. Structurally, the shorter distance to the next drill bearing, the greater the bit side force and stronger the buildup ability.

(3) The location of the point of the biasing force greatly influences the bit lateral force. Therefore, the tool can be designed to position the biasing force to increase buildup ability.

(4) The results of this research provide a basis for the design of bearing loads and operations.

(5) This paper discusses only the structural parameter optimization and buildup ability choice of point-the-bit RSS.

4. ELASTIC STABILITY QUESTION ON TWO-SPAN CONTINUOUS BEAMS

4.1 Research on Elastic Stability of Compressed Bar for Two-Span Continuous Beams and Its Application in the Rotary Steerable Drilling Tools

While studying RSS mechanical performance, an essential factor should be taken into consideration. That is the effect of the tools elastic stability on the tools mechanical performance under axial loading with present structural conditions. In view of the tools structural characteristics, we can know the limit of tools elastic stability with weight-on-bit conditions, i.e. what are the weight-on-bit or critical values of axial loading for elastic stability. This will reduce unnecessary loss because of improper design or operation of the tools. Therefore, it is very important to continue research on tools elastic stability characteristics.

4.1.1 Problems

Since the introduction of point-the-bit RSS tools, it has been widely applied, especially for directional wells, horizontal wells and multi-lateral wells. This shows the RSS advantages such as strong built-up ability, easiness of operation and higher adaptability. However, with strength on tools adaptability, application range is widely extended. KOP depth in vertical wells becomes more shallow, and requirements for the built-up rate becomes higher [30] [31] [32]. Geo-pilot introduced by Halliburton has the ability of built-up in 26 inch wellbore, while used with 11-3/4 inch and 9-5/8 inch mud motors, that is, the dimension of our point-the-bit RSS tools can cover regular wellbore dimensions commonly used in offshore operations. Today's drilling methods, demand

higher efficiency, faster ROP and shorter drilling footage time. So we should know the maximum weight-on-bit that could be exerted on this tool system. In other words we need higher ROP but suitable weight-on-bit, to avoid damaging the tool. Therefore, research on elastic stability of the tool systems is very important and will ensure reasonable operation and protection as well as increasing ROP.

4.1.2 Mechanic model establishment

Combined with the structural characteristics of point-the-bit RSS and real operational conditions, the tool system consists of: (1) bit, (2) adjustable stabilizer; (3) drilling stem; (4) middle stabilizer; (5) drilling string; (6) upper stabilizer. Point-the-bit RSS structure is shown in figure 4.1.

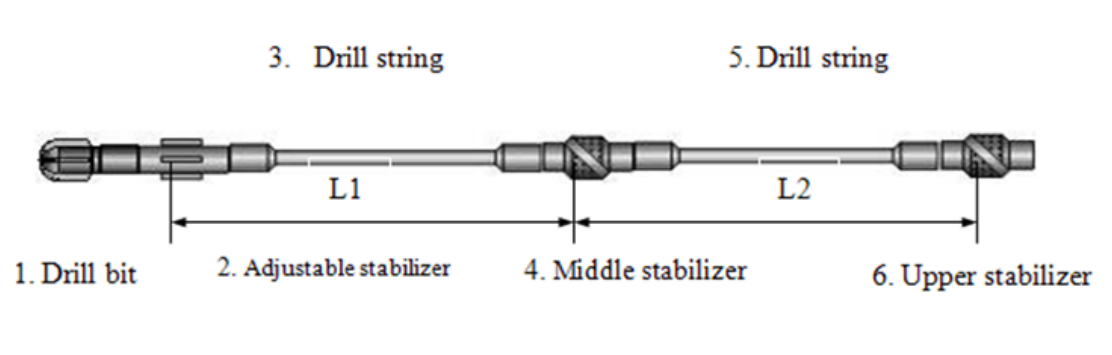

Figure 4.1 Point-the-Bit Rotary Steerable Drilling Tool System

Coordination system established along axial direction of drilling string and for simplification, some assumption taken as follows:

1. Mass of drilling string is continuously distributed, that is taking no consideration of changing mass and stiffness effect.

2. Stiff wellbore, taking no consideration of enlargement of the wellbore.

3. Making contact between adjustable stabilizer, stabilizer and wellbore as hinge support.

4. Considering the effect of axial loading on the tool system's elastic stability, taking no consideration of lateral loading, mainly focus on elastic stability problems before initial KOP point.

Therefore, the tool system mechanic model can be obtained as Figure 4.2.

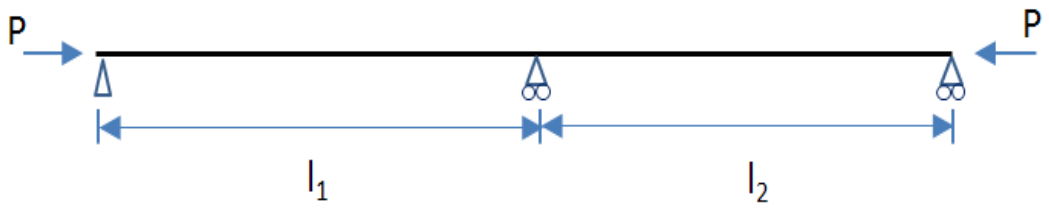

Figure 4.2 Configuration of Rotary Steerable Drilling System

Also we have studied stress problems of the RSS, but we need to continue discussing the elastic stability problems for two-span continuous beams with three supporting points.

1. If $\ell_1 = \ell_2 = \ell$, middle supporting located at point of curved plane, moment of this point is zero as figure 3, its critical pressure PE could be derived from literature [33] [34] as:

$$P_E = \frac{\pi^2 EJ}{l^2} \tag{4.1}$$

That is typical Euler loading for stable compressed bar. The mechanical model of two-span continuous beam is shown in Figure 4.3.

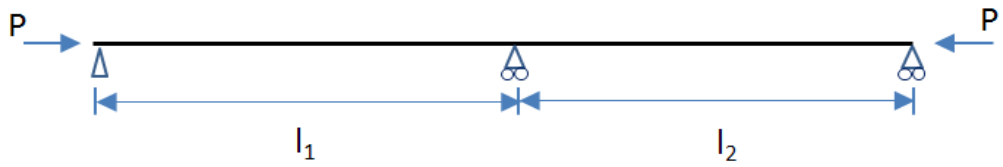

Figure 4.3 Two-Span Continuous Beam Models with Same Intervals

2. More scenario we met across in BHA could be as: because of different of requirements of built-up capacity and tools design structure, $\ell_1 \neq \ell_2$, more stiffness span could transfer to less stiffness span, which increase more elastic stability, therefore, moment could not be zero at the point of middle supporting, we could obtain the solution from following formula:

$$EJy'''' + Py'' = q(x) \tag{4.2}$$

Character value of above equation could be solved, let q(x) =0 and $y = Ae^{\lambda x}$, substitute into equation (4.2), then:

$$\lambda^4 + \alpha^2 \lambda^2 = 0 \tag{4.3}$$

$$\lambda^2 \left(\lambda^2 + \alpha^2\right) = 0 \tag{4.4}$$

Where, $\alpha = \frac{P}{EJ}$ double root could be solved by above formula [33] [35] [36]:

$$\lambda_1 = \lambda_2 = 0 \tag{4.5}$$

$$\lambda_3 = \lambda_4 = \pm i\alpha \tag{4.6}$$

$$y = A_1 + A_2 i\alpha x + A_3(\cos\alpha x + i\sin\alpha x) + A_4(\cos\alpha x - i\sin\alpha x)$$

$$y = A_1 + A_2 i\alpha x + (A_3 + A_4)\cos\alpha x + i(A_3 - A_4)\sin\alpha x$$

$$y = C_0 + C_1\alpha x + C_2\cos\alpha x + C_3\sin\alpha x \tag{4.7}$$

Confirm the indeterminate coefficient by boundary conditions:

$$\text{x} = 0, \quad y_0 = 0, \quad y'' = \frac{M_1}{EJ}$$

$$\text{x} = l, \quad y_1 = 0, \quad y_1'' = \frac{M_2}{EJ}$$

Substitute into formula (4.6):

$$C_2 = -C_0 \tag{4.8}$$

Differentiation of formula (4.7), then:

$$y' = C_1\alpha - C_2\alpha\sin\alpha x + C_3\alpha\cos\alpha x$$

$$y'' = -C_2\alpha^2\cos\alpha x - C_3\alpha^2\sin\alpha x$$

$\because \ x = 0 \ \ y_0'' = \frac{M}{EJ}$ Substitute into above formula:

$$\frac{M_1}{EJ} = -\text{C}_2\alpha^2 \quad \therefore \quad \text{C}_2 = -\frac{\text{M}_1}{EJ\alpha^2} \tag{4.9}$$

Substitute formula (4.8) into (4.9), then $\text{C}_0 = \frac{\text{M}_1}{EJ\alpha^2}$ (4.10)

Similarly, when $x = l$, $y_1 = 0$ substitute into formula (4.7), then:

$$0 = \frac{\mathrm{M}_1}{EJ\alpha^2} + C_1\alpha l - \frac{M_1}{EJ\alpha^2}\cos\alpha l + C_3 \sin\alpha l$$

$$0 = \frac{\mathrm{M}_1}{EJ\alpha^2}(1-\cos\alpha l) + C_1\alpha l + C_3 \sin\alpha l \tag{4.11}$$

And $\because\ y_1'' = \frac{M_2}{EJ} = -\mathrm{C}_2\alpha^2\cos\alpha x - C_3\alpha^2 \sin\alpha x$

$$\frac{M_2}{EJ} = \frac{M_1}{EJ\alpha^2}\alpha^2\cos\alpha l - C_3\alpha^2 \sin\alpha l$$

$$C_3 = \left(\frac{M_1}{EI\alpha^2}\alpha^2\cos\alpha l - \frac{M_2}{EI}\right)\frac{1}{\alpha^2\sin\alpha l} = \frac{1}{\alpha^2\sin\alpha l EI}(M_1\cos\alpha l - M_2) \tag{4.12}$$

Therefore, substitute C_1, C_2, C_3 and C_0 into formula (4.7), then:

$$y(x) = \frac{M_1}{EJ\alpha^2}\left[-\frac{\sin\alpha(l-x)}{\sin\alpha l} + \frac{\alpha(l-x)}{\alpha l}\right] + \frac{M_2}{EJ\alpha^2}\left(\frac{\alpha x}{\alpha l} - \frac{\sin\alpha x}{\sin\alpha l}\right) \tag{4.13}$$

$$y'(x) = \frac{M_1}{EJ\alpha}\left[\frac{\cos\alpha(l-x)}{\sin\alpha l} - \frac{1}{\alpha l}\right] + \frac{M_2}{EJ\alpha}\left(\frac{1}{\alpha l} - \frac{\cos\alpha x}{\sin\alpha l}\right) \tag{4.14}$$

$$y''(x) = \frac{M_1}{EJ\alpha}\left[\frac{\alpha\sin\alpha(l-x)}{\sin\alpha l}\right] + \frac{M_2}{EJ\alpha}\left(\frac{\alpha\sin\alpha x}{\sin\alpha l}\right) \tag{4.15}$$

Set $\psi = 2u$, $\frac{1}{2}\alpha l = u$ and introduce symbol:

$$\psi(u) = \frac{3}{2u}\left(\frac{1}{2u} - \frac{1}{tg\,2u}\right) \tag{4.16}$$

$$\phi(u) = \frac{6}{2u}\left(\frac{1}{\sin 2u} - \frac{1}{2u}\right) \tag{4.17}$$

Substitute formula (4.16) and (4.17) into formula (4.14), then:

$$
\begin{aligned}
y'_{(0)} &= \frac{M_1}{EJ\alpha}\left[\frac{\cos\alpha l}{\sin\alpha l}-\frac{1}{\alpha l}\right]+\frac{M_2}{EJ\alpha}\left(\frac{1}{\alpha l}-\frac{1}{\sin\alpha l}\right) \\
&= \frac{M_1}{EJ\alpha}\left[\frac{1}{tg2u}-\frac{1}{2u}\right]+\frac{M_2}{EJ\alpha}\left(\frac{1}{2u}-\frac{1}{\sin 2u}\right) \\
&= -\frac{M_1 l}{EJ\cdot 2u}\left[\frac{1}{2u}-\frac{1}{tg2u}\right]-\frac{M_2 l}{EJ\,2u}\left(\frac{1}{\sin 2u}-\frac{1}{2u}\right)
\end{aligned}
$$

$$
\begin{aligned}
y'_{(0)} &= -\frac{M_1 3l}{3EJ\cdot 2u}\left[\frac{1}{2u}-\frac{1}{tg2u}\right]-\frac{6M_2 l}{6EJ\,2u}\left(\frac{1}{\sin 2u}-\frac{1}{2u}\right) \\
&= -\frac{M_1 l}{EJ}\psi(u)-\frac{M_2 l}{6EJ}\phi(u)
\end{aligned}
\tag{4.18}
$$

While, from formula (4.14), we could know:

$$
\begin{aligned}
y'_{(l)} &= -\frac{M_1}{EJ\alpha}\left[\frac{1}{\sin\alpha l}-\frac{1}{\alpha l}\right]+\frac{M_2}{EJ\alpha}\left(\frac{1}{\alpha l}-\frac{\cos\alpha l}{\sin\alpha l}\right) \\
&= \frac{M_1 l}{EJ\,2u}\left[\frac{1}{\sin 2u}-\frac{1}{2u}\right]+\frac{M_2 l}{EJ\,2u}\left(\frac{1}{2u}-\frac{1}{tg2u}\right) \\
&= \frac{6M_1 l}{6EJ\,2u}\left[\frac{1}{\sin 2u}-\frac{1}{2u}\right]+\frac{3M_2 l}{3EJ\,2u}\left(\frac{1}{2u}-\frac{1}{tg2u}\right) \\
&= \frac{M_1 l}{6EJ}\phi(u)+\frac{M_2 l}{3EJ}\psi(u)
\end{aligned}
\tag{4.19}
$$

$$
\text{Where, } u_1 = \frac{l_1}{2}\sqrt{\frac{P}{EJ}} \quad u_2 = \frac{l_2}{2}\sqrt{\frac{P}{EJ}} \tag{4.20}
$$

Supposing the rotating angle at left and right side are same at the middle of supporting point, that is, formula (4.18) equals to formula (4.19).

$$
\therefore -\frac{M_l l_1}{3EJ}\psi(u_1)-\frac{M_2 l_1}{6EJ}\phi(u_1)=\frac{M_l l_2}{6EJ}\phi(u_2)+\frac{M_2 l_2}{3EJ}\psi(u_2)
$$

Considering Symmetry, when x=0, M_2 at B point equals to zero, and when x=l, M_1 at A point equals to zero.

$$\therefore \; -\frac{\mathrm{M}_1 l_1}{6EJ}\psi(u_1) = \frac{\mathrm{M}_l l_2}{6EJ}\phi(u_2)$$

$$-\frac{\mathrm{M}_l l_1}{3EJ}\psi(u_1) = -\frac{\mathrm{M}_2 l_2}{3EJ}\phi(u_2) \tag{4.21}$$

Where, $u_1 = \frac{l_1}{2}\sqrt{\frac{P}{EJ}}$, $u_2 = \frac{l_2}{2}\sqrt{\frac{P}{EJ}}$, $M_1 = M_2 = M$

From formula (4.21) we can get:

$$\frac{\mathrm{M}l_1}{3EJ}\psi(u_1) = -\frac{\mathrm{M}l_2}{3EJ}\phi(u_2)$$

$$\therefore \; M\left[l_1\psi(u_1) + l_2\psi(u_2)\right] = 0 \tag{4.22}$$

When $M \neq 0$, then:

$$l_1\psi(u_1) + l_2\psi(u_2) = 0$$

Combined with formula (4.16), then:

$$l_1 \cdot \frac{3}{2u_1}\left(\frac{1}{2u_1} - \frac{1}{tg\,2u_1}\right) = -l_2 \cdot \frac{3}{2u_2}\left(\frac{1}{2u_2} - \frac{1}{tg\,2u_2}\right)$$

$\because \; \alpha l = 2u$, $\therefore \; \frac{2u}{l} = \alpha$

$\therefore$ Substitute into above formula, then:

$$\frac{3}{\alpha}\left(\frac{1}{2u_1} - \frac{1}{tg\,2u_1}\right) = -\frac{3}{\alpha}\left(\frac{1}{2u_2} - \frac{1}{tg\,2u_2}\right)$$

$$-\left(\frac{1}{2u_1} - \frac{1}{tg\,2u_1}\right) = -\left(\frac{1}{2u_2} - \frac{1}{tg\,2u_2}\right) \tag{4.23}$$

$\therefore$ The critical pressure for continuous beam could determined by above transcendental equations, introducing symbol $\Phi(2u_1) = \dfrac{tg2u - 2u}{2utg2u}$

$$\frac{tg2u_1 - 2u_1}{2u_1 tg2u_1} = -\frac{tg2u_2 - 2u_2}{2u_2 tg2u_2} \tag{4.24}$$

$$\therefore \Phi(2u_1) = -\Phi(2u_2) \tag{4.25}$$

Considering period of the trigonometric function, set 2u within the range of 0 to 2, therefore, we could calculate the periodic function (case 1) shown in Table 4.1.

Table 4.1 Periodic Function Calculation in Case 1

2u	0.1*л	0.2*л	0.3*л	0.4*л	0.5*л	0.6*л	0.7*л	0.8*л	0.9*л	л
2u	0.3142	0.6283	0.9425	1.256	1.57	1.884	2.198	2.512	2.8274	3.14
ϕ(2u)	0.11	0.22	0.33	0.47	0.64	0.85	1.18	1.77	3.43	628.20
2u	1.1*л	1.2*л	1.3*л	1.4*л	1.5*л	1.6*л	1.7*л	1.8*л	1.9*л	2*л
2u	3.454	3.768	4.082	4.396	4.71	5.024	5.338	5.652	5.966	6.28

From above we know, $\alpha l = 2u$

$$\therefore \alpha = \frac{2u}{l} = \frac{2u_1}{l_1} = \frac{2u_2}{l_2}$$

$$\therefore 2u_2 = \frac{l_2}{l_1} 2u_1$$

Let $\ell_1 > \ell_2$, then $2u_1 = \dfrac{l_1}{l_2} 2u_2 = \alpha l_1$ (4.26)

Similarly, $2u_2 = \alpha l_2$ (4.27)

$$\therefore \frac{2u_2}{2u_1} = \frac{\alpha l_2}{\alpha l_1} = \frac{l_2}{l_1} \tag{4.28}$$

Determine the minimum roots of formula (4.24), from formula (4.20), we could get:

$$\because u = \frac{l}{2}\sqrt{\frac{P}{EJ}} \longrightarrow P = EJ\left(\frac{2u}{l}\right)^2$$

$$\therefore \text{The critical pressure: } P_{cr_1} = EJ\left(\frac{2u_1}{l_1}\right)^2 \tag{4.29}$$

$$P_{cr_2} = EJ\left(\frac{2u_2}{l_2}\right)^2 \tag{4.30}$$

$\because 2u_2 = \frac{l_2}{l_1}2u_1$, $\therefore$ when $\ell_1 > \ell_2$, $2u_1 > \pi$, $2u_2 < \pi$, so the critical pressure should be as follows:

$$\frac{\pi^2 EJ}{l_2^{\,2}} > P_E > \frac{\pi^2 EJ}{l_1^{\,2}}$$

Obviously, at the position of critical point, the same results could be obtained, thus, we get the solutions for critical pressure of dual span continuous beam under continuous supporting conditions.

4.1.3 Solutions and case studies

Considering real conditions of drilling tools, generally, rotary steerable drilling tools length is shorter than length of drilling collar assembly for measurement while drilling tools, therefore, we can take assumptions as $\ell_1 > \ell_2$, and $\ell_1 = 2\ell_2$, and from formula (4.28), we could obtain:

$$\frac{2u_2}{2u_1} = \frac{l_2}{l_1} = \frac{l_2}{2l_2} = \frac{1}{2}$$

$$\therefore 2u_2 = u_1$$

From formula (4.25), $\Phi(2u_1) = -\Phi(2u_2) = -\Phi(u_1)$, that is $\Phi(2u_1) = -\Phi(u_1)$ (4.31)

$$\frac{tg2u_1 - 2u_1}{2u_1 tg2u_1} = -\frac{tgu_1 - u_1}{u_1 tgu_1} \quad (4.32)$$

Based on Table 4.1, we could determine the value of $\Phi(2u_1)$ and get Table 4.2. According to Table 4.1, we could get two curves as $\Phi(2u)$ and $2u_1$, then get another curve as $2u_2$ and $-2u_2$. We could calculate the periodic function (case 2) shown in Table 4.2. The curve for determining minimum root is shown in Figure 4.4.

Table 4.2 Periodic Function Calculation in Case 2

2u	**0.1*л**	**0.2*л**	**0.3*л**	**0.4*л**	**0.5*л**	**0.6*л**	**0.7*л**	**0.8*л**	**0.9*л**	**л**
2u	0.314	0.628	0.942	1.256	1.57	1.884	2.198	2.512	2.827	3.14
ф(2u1.)	0.11	0.22	0.33	0.47	0.64	0.85	1.18	1.77	3.43	628.20
ф(2u2.)	0.05	0.11	0.16	0.22	0.27	0.33	0.40	0.47	0.55	0.64
ф(-2u2.)	-0.05	-0.11	-0.16	-0.22	-0.27	-0.33	-0.40	-0.47	-0.55	-0.6
2u	**1.1*л**	**1.2*л**	**1.3*л**	**1.4*л**	**1.5*л**	**1.6*л**	**1.7*л**	**1.8*л**	**1.9*л**	**2*л**
2u	3.454	3.768	4.082	4.396	4.71	5.024	5.338	5.652	5.966	6.28
ф(2u1.)	-2.81	-1.12	-0.48	-0.10	0.21	0.52	0.91	1.55	3.21	314.10
ф(2u2.)	0.74	0.85	1.00	1.18	1.42	1.77	2.33	3.42	6.59	628.20

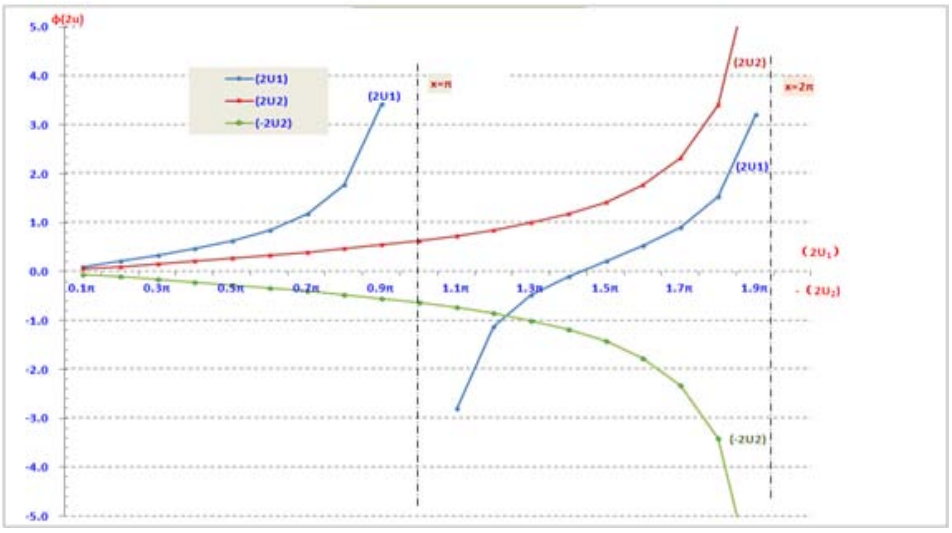

Figure 4.4 Curve for Determining Minimum Root

From Figure 4.4 we can know the cross point of $2u_2$ and $-2u_2$ is the minimum root. The transcendental equations above can be calculated by trial method, we can know the cross point position is $2u_1=1.25\pi$, so set $2u_1=1.2\pi$, check Table 4.4 we get $\Phi(2u_1)=-1.11$, select value from Table 4.1, half of 1.2π is 0.6π, $2u_2=0.6\pi$, $\Phi(2u_2)=0.855$, attention that $\Phi(2u_1)$ is positive at that time, then select $2u_1=1.4\pi$, then $\Phi(2u_1)=0.097$. When

$2u_2=0.7\pi$, $\Phi(2u_1)=1.81$

$2u_2=1.3\pi$, $\Phi(2u_1)=-0.482$

$2u_2=0.65\pi$, $\Phi(2u_1)=0.855\sim1.181$

Therefore, $1.3\pi<2u_1<1.4\pi$ that is, $2u_1$ within the range of -0.482 and 0.097

Critical pressure: $P_{cr} = EJ\left(\frac{2u_1}{l_1}\right)^2$ (4.33)

Observation of formula (4.33), we can find:

(1) The magnitude of critical loading P_E is in proportion to bending module EJ and is inversely proportion to square of the length of beam.

(2) If $2u_1=\pi$, the formula (4.33) can be transformed to $P_{cr} = rEJ\left(\frac{\pi}{l_1}\right)^2$, which is obviously a critical value expression of standard Euler loading for hinge at both end [33] [37].

(3)In this case, $1.3\pi<2u_1<1.4\pi$, the critical value for loading is more higher, which is the difference between single span beam hinge at both end and two span beam hinge at both end.

4.1.4 Calculations

[Example 1] assumption dimension for rotary steerable drilling tools is know, outer diameter and inner diameter is taken according to API standard as follows:

(1) 6-1/2" OD is 0.165m, ID is 0.0714m

(2)7" OD is 0.1778m, ID is 0.0714m

(3)8" OD is 0.2030m, ID is 0.0714m

(4)9" OD is 0.2236m, ID is 0.0762m

Determine: when ℓ_2 is 7m, ℓ_1 is 19m, 27m and 36m, the value of critical loading P_E

Solution: according to derivation method in this paper, list result into Table 4.3, several declarations show as follows:

- For simplification, it's more convenience to calculate transcendental equations by iteration method.
- Data shown in Table 4.3 is standard configuration for API drilling collar dimension.
- Considering contrasting and observation, for the sake of finding changing regulation of critical loading, two kinds thickness is used in Table 4.3, which 2.68cm is for 6-1/2" and 7" drilling stem, and 3.32cm is for 8" and 9" drilling stem.
- Combined with current configuration conditions for RSS tools, we take an assumption that ℓ_2=7m is fixed, and then adjusting the length of ℓ_1, the changing regulation of critical loading P_E can shown in Table 4.3.
- From Table 4.3, for the same outer diameter drilling collar, when ℓ_2 is unchanged, with the increasing of ℓ_1, critical loading P_E would be decreased, such as, for 6-1/2" DC, when ℓ_2 increase from 27m to 36m, the critical loading will decrease from 17.5t to 10.2t, that is, when the length increased 3 times, critical loading decreased 26%-28%.
- From Table 4.3, with the same span, the more geometry dimension of drilling stem, the more critical loading, for an instance, when mandrel length= 18 m, 6-1/2" DC critical loading is 36 t, but for 7" DC, the critical loading would be 49.5 t, for 8" DC is 85 t, 9" DC is 125 t, if outer diameter increase 1", critical loading would increase 72%-47%.
- From Table 4.3, with the same thickness, when outer diameter increasing, critical

loading will corresponding increase, for example, if thickness is 2.68 cm, for 7”DC, the critical loading would be 38.7 t when mandrel length= 18 m, however, for 6-1/2”DC, critical loading would be 29 t under the same conditions, increased 33%.

- From Table 4.3, if the thickness changed to 3.32 cm, the critical loading for 9”DC would be higher than that of 8” DC, could arrive at 95.9 t, increase 39.7%.
- When inner diameter is same, the critical loading for different out diameter DC is shown in Table 4.3, general changing regulation is the same as above.

4.1.5 Conclusion and reorganization

1. It is very important to study the critical weight-on-bit for RSS utilizing the methods in this paper. This would be helpful for us to select reasonable drilling parameters for assessing the elastic stability of the drilling system.

2. Compared with traditional Euler loading hinge at both ends, the value calculated in the paper would be larger, mainly because middle support exists, enhancing elastic stability and increasing critical loading.

3. Elastic stability for RSS tools is discussed in view of these research results. Because more axial loading is exerted on the lower BHA, the analysis of this load is essential for safe operations.

4. Regarding the elastic stability for lower BHA, more attention should be paid to the fact that Euler loading hinge at both ends could not be simply used to analyze this problem, because of continuous supporting compressed bar, different conditions could give different values. The Critical Load for API is shown in Table 4.3.

Table 4.3 the Critical Load for API Standard Drill Collar

	OD m	ID M	δcm	J M4	L1 m	L2 m	Pcr Kkg
61/2"	0.165	0.0714	4.68	3.509E-05	36	7	10.2
61/2"	0.165	0.0714	4.68	3.509E-05	27	7	17.5
61/2"	0.165	0.0714	4.68	3.509E-05	18	7	36.0
7"	0.1778	0.0714	5.32	4.776E-05	36	7	13.9
7"	0.1778	0.0714	5.32	4.776E-05	27	7	23.8
7"	0.1778	0.0714	5.32	4.776E-05	18	7	49.5
8"	0.2032	0.0714	6.59	8.237E-05	36	7	23.9
8"	0.2032	0.0714	6.59	8.237E-05	27	7	41.0
8"	0.2032	0.0714	6.59	8.237E-05	18	7	85.0
9"	0.2236	0.0762	7.37	0.000121	36	7	33.1
9"	0.2236	0.0762	7.37	0.000121	27	7	60.2
9"	0.2236	0.0762	7.37	0.000121	18	7	125.0
61/2"	0.165	0.1114	2.68	2.881E-05	36	7	8.4
61/2"	0.165	0.1114	2.68	2.881E-05	27	7	14.3
61/2"	0.165	0.1114	2.68	2.881E-05	18	7	29.0
7"	0.1778	0.1242	2.68	3.736E-05	36	7	10.8
7"	0.1778	0.1242	2.68	3.736E-05	27	7	18.6
7"	0.1778	0.1242	2.68	3.736E-05	18	7	38.7
8"	0.2032	0.1368	3.32	6.646E-05	36	7	19.3
8"	0.2032	0.1368	3.32	6.646E-05	27	7	33.1
8"	0.2032	0.1368	3.32	6.646E-05	18	7	68.8
9"	0.2236	0.1572	3.32	9.268E-05	36	7	26.9
9"	0.2236	0.1572	3.32	9.268E-05	27	7	46.1
9"	0.2236	0.1572	3.32	9.268E-05	18	7	95.9
61/2"	0.165	0.1114	2.68	2.881E-05	36	7	8.4
61/2"	0.165	0.1114	2.68	2.881E-05	27	7	14.3
61/2"	0.165	0.1114	2.68	2.881E-05	18	7	29.0
7"	0.1778	0.1114	3.32	4.148E-05	36	7	12.0
7"	0.1778	0.1114	3.32	4.148E-05	27	7	20.0
7"	0.1778	0.1114	3.32	4.148E-05	18	7	42.9
8"	0.2032	0.1114	4.59	7.609E-05	36	7	22.1
8"	0.2032	0.1114	4.59	7.609E-05	27	7	37.8
8"	0.2032	0.1114	4.59	7.609E-05	18	7	78.7
9"	0.2236	0.1114	5.61	0.0001151	36	7	33.0
9"	0.2236	0.1114	5.61	0.0001151	27	7	57.2

5. CONCLUSIONS

Minimizing investments in exploration and development and reducing the cost per ton of crude oil have become important concerns in offshore and onshore oil and gas exploration and development. At present, the technologies of directional, horizontal and extended reach wells have been the preferred methods for oil and gas field development. Use of these drilling technologies can increase the drainage area per well, while the total cost is reduced by decreasing the investment in drilling platforms and artificial islands. Realization of these drilling technologies relies on advanced RSS technology and tool systems. From this study, we draw several conclusions and recommendations.

(1) RSS technology is a powerful tool for oil exploration and development. It effectively solves technical difficulties in oil and gas exploration and development. Particularly, with regard to higher productivity and fewer drilling risks and downhole accidents with more exposed reservoirs, it delivers excellent performance. It is playing an increasingly important role in global oil and gas exploration and development.

(2) A basic theoretical study of a rotary steering tool system helps us further master the mechanical characteristics of the tool system from the angle of mechanical behavior and features of the tool. In combination with different whipstocking operation principles, we have established different mechanical models to solve the mechanical property parameters, and we made assessed the mechanical properties and features of the RSS using multiple approach.

(3) With a view to the current practical application of rotary steering drilling tools, we conducted intensive exploration and theoretical analysis of the tool system's bit

side force and the influence of the bias unit's concentrated load and biased load on the side force. Results of this research serve as reference points for our study of tool design and mechanical structure.

(4) To rationalize the tool's stress state and ensure that the tool system can both obtain ideal side force and reasonably bear the influence of biased load and side force on bearing stress at bearing support, we assessed the active position of biased load, the mandrel length, the extended length. All of these mainly contribute to and are reflected in the design and usage and should be considered in design and application.

(5) A rotary steering tool integrating electronic measurement and mechanical action is fully functional, structurally complex and expensive. Therefore, from the perspective of dynamics, we conducted a basic theoretical study of the dynamic characteristics of the tool system, especially for the natural frequency, to guide design and actual oil field operation and effectively avoid the resonant frequency and resonant speed of common drilling tools. The study goal was to ensure that tool design avoided damage and also extend the tool service life effectively.

(6) In general, the RSS performs well in actual operations, as a mainstream technology in the oil field exploration and development. This technology has played an increasingly important role in the oil industry.

In the application of such new technologies as multilateral, horizontal and extended reach wells, RSS technology has brought significant economic benefits. In the field of oil industry technology, RSS fully embodies the reform and great change in oil field drilling technologies. Because of the perfect embodiment of these advanced

technologies, RSS technology demonstrates oil field development technical and economic advantages. We recommend continued research of the technical characteristics and working mechanisms of RSS, owing to the practical significance for the engineering applications, and the economic significance and far-reaching impacts on oil recovery from increasingly complex wells and reservoirs.

NOMENCLATURE

E	elastic module, MPa
J	polar moment of inertia, cm^4
P	concentrated load caused by offset wheel, N
P_{cr}	the critical loading for the drill string, N
R_A	reaction force at upper bearing, N
R_B	reaction force at lower bearing, N
R_C	reaction force at the bit or side force on the bit, N
y	mandrel deflection under bias loading, cm
ℓ	length of mandrel, cm
c	distance between drill bit and lower bearing, cm
Q	bit side force, N
λ	axial offsetting, cm
A	area of the mandrel section, cm^2
σ	tension stress, kg/cm^2
α	angle of well bore inclination, degree
q	weight of the mandrel per unit length, kg/m
ω	natural frequency, sec^{-1}
Nn	resonance rotation speed of the point-the-bit RSS tools, rpm
M	mass of point loading, N
g	gravity acceleration, cm/sec^2
b	distance from concentrated load to the upper supporting, cm

δ	static deflection of the central spindle, cm
a	distance from drill bit to bias concentrated load, cm
ℓ_2	distance between lower stabilizer and middle stabilizer, m
ℓ_1	distance between middle stabilizer and upper stabilizer, m

REFERENCES

[1] Travis, J. T. Jr., Moss, J. H., and Browning, G. M.: "An Operators Targeted Development of Low-Cost 3D Rotary Steerable Systems", IADC/SPE 87165, presented at the 2004 IADC/SPE Drilling Conference, Dallas, TX, 2-4 March, 2004.

[2] Porter D.S. and Al-Faraj, H.: "Rotary-Steerable Technology Proves to be Economically Successful in Offshore Arabia Gulf Fields," paper SPE 85339 presented at the 2003 IADC/SPE Middle East Drilling Technology Conference & Exhibition, Abu Dhabi, UAE, 20–22 October.

[3] Molayee, A., and A. Teymoori, 2006. "Experience with Rotary Steerable Systems for Reservoir Drilling in Iranian Offshore Oil fields." Paper SPE 100917 presented at the Asia Pacific Oil & Gas Conference and Exhibition held in Adelaide, Australia, 11-13 September 2006.

[4] Stroud, D., Russell, M., and Peach, S.: "Development of the Industry's First Slimhole Point-the Bit Rotary Steerable System," paper SPE 84449 presented at the 2003 SPE Annual Technical Conference and Exhibition, Denver, Colorado, USA, 5-8 October.

[5] Sugiura, J., and Jones, S.: "Integrated Approach to Rotary-Steerable Drilling Optimization Using Concurrent Real-time Measurement of Near-bit Borehole Caliper and Near-bit Vibration", SPE 112163 presented at the 2008 SPE Intelligent Energy Conference and Exhibition, Amsterdam, The Netherlands, 25-27 February 2008.

[6] Cox, B. and Naganathan, S.: "High Dogleg Rotary Steerable System: A Step Change in Drilling Process". Paper SPE 124498 presented at the Annual Technical Conference and Exhibition, 4-7 October, 2009.

[7] Pratten, C., El Kholy, K., Nagamathan, S., and Sharaf, E.: "Rotary Steerable System Applications in the Middle East," paper SPE 85285, presented at the 2003 IADC/SPE Middle East Drilling Technology Conference & Exhibition, Abu Dhabi, UAE, 20–22 October.

[8] Sugiura, J.: "The Use of the Near-bit Vibration Sensor While Drilling Leads to Optimized Rotary-Steerable Drilling in Push- and Point-the-Bit Configurations", SPE 115572 presented at the 2008 Asia Pacific Oil & Gas Conference and Exhibition, Perth, Australia, 20-22 October 2008.

[9] Kuyken, C., Plas, K., Frederiks, K., Williams, M., Cockburn, C.: "Developing and Using Slimhole Rotary Steerable Systems in the North Sea Changing the Economics of Mature Asset Drilling", paper SPE 83948 presented at Offshore Europe 2003 held in Aberdeen, Scotland, U.K. 2-5 September 2003.

[10] Jones, S., and Sugiura, J.: "Concurrent Rotary-Steerable Directional Drilling and Hole Enlargement Applied Successfully: Case Studies in North Sea, Mediterranean Sea and Nile Delta", SPE 112670 presented at the 2008 IADC/SPE Drilling Conference, Orland, Florida, 4-6 March 2008.

[11] Moody, M., Jones, S., and Leonard, P.: "Development and Field Testing of a Cost-Effective Rotary Steerable System", SPE 90482 presented at the SPE Annual Technical Conference and Exhibition, Houston, Texas, 26-29 September 2004.

[12] Barton ,S., Garcla, A., Luther, C., and Noriega, I.: "Unique string tools combine to save over USD 11 million in challenging hole opening rotary-steerable applications". SPE 124352 presented at the CPS/SPE international Oil & gas conference and exhibition, Beijing, China, 8–10 June 2010.

[13] Baker Hughes, "http://www.bakerhughes.com/products-and-services/drilling/drilling-services/directional-drilling-services/rotary-steerable-systems."

[14] Schlumberger, "http://www.slb.com/services/drilling/drilling_services_systems/directional_drilling/powerdrive_family.aspx."

[15] Halliburton, "http://www.halliburton.com/en-US/ps/sperry/drilling/directional-drilling/rotary-steerables/solar-geo-pilot-xl-rotary-steerable-system."

[16] Al-Suwaidi, A., Allen, F., Taylor, R., Hussein, K. and Russell, R., "Experience with Rotary Steerable Systems in Onshore Abu Dhabi Fields", SPE/IADC 85291 presented at the AE/IADC Middle East Drilling Conference and Exhibition, Abu Dhabi, U.A.E., 20-22 Oct, 2003.

[17] Shan, J.: "Flexural Distortion Analysis of the Mandrel in an Orienting Rotary Steerable Drilling Tool". SPE 136727 presented at the CPS/SPE international Oil & gas conference and exhibition, Beijing, China, 8–10 June 2010.

[18] Jiansheng, D., Baolin, L.,Qingtao, L., and Xiaojun, H.: "The mechanical model establishment and optimization of the rotary shaft in the point-the-bit rotary steerable drilling system". China Petroleum Machinery; 2008, Vol.36 No 8, P28-31.

[19] Liankun Li editor in chief ,Hunan University, Southwest Jiaotong University, Changsha Railway University , eds, Structural Mechanics. People's Education Press, Beijing, 1979, pp. 265.

[20] Gere JM, Timoshenko S (1997) in Mechanics of Materials (PWS Pub. Co., Boston), 4th Ed, pp 560-561.

[21] Hernan, M., Grace, W., Gonzalez, L., Alric, C., Palacio, J., Akinniranye, G.: "Remote Automated Directional Drilling Through Rotary Steerable Systems". SPE 119761, presented at the SPE/IADC Drilling Conference and Exhibition, 17-19 March, Amsterdam, The Netherlands, 2009.

[22] S., Cox, J., Blackwell, D., Slayden, W., Naganathan, S.: "High-Dogleg Rotary-Steerable Systems: A Step Change in Drilling Process". SPE 124498, presented at the SPE Annual Technical Conference and Exhibition, New Orleans, Louisiana, USA, 4-7 October, 2009

[23] Porter D.S. and Al-Faraj, H.: "Rotary-Steerable Technology Proves to be Economically Successful in Offshore Arabia Gulf Fields". SPE 85339, presented at the IADC/SPE Middle East Drilling Technology Conference & Exhibition, Abu Dhabi, UAE, 20–22 October, 2003.

[24] Malik, M., Tewari, R., Naganathan, S.: "Rotary Steerable Systems Results in Step Change in Drilling Performance-A Case Study". SPE 103842, presented at the IADC/SPE Asia Pacific Drilling Technology Conference and Exhibition, 13-15 November, Bangkok, Thailand, 2006.

[25] Hongwen, L (2004) in Mechanics of Materials (Higher Education Press, Beijing), 4th Edition, pp 175-180.

[26] Timoshenko, S., Gere, JM (1965) in Elastic Stability Theory (Science Press, Beijing), Zhang Fufan translation, second edition, pp 30-33.

[27] Timoshenko, S. (1972) Mechanics of Materials, (Van Nostrand Reinhold Company), Hu Renli translation, (Science Press, Beijing), pp 311-313.

[28] Timoshenko, S., Gaelic, J. Mechanics of Materials, 1st Edition, (Science Press, Beijing), Hu Renli translation, March 1978, pp 216-224.

[29] S Timoshenko. Mechanics of Materials (advanced theory and question), SH Tang translation, Science Press, Beijing, 1979, pp 42-51.

[30] Downton, G.C. and Carrington, D.: "Rotary Steerable Drilling System for 6-in Hole," SPE 79922, presented at the SPE/IADC Drilling Conference, 19-21 February, Amsterdam, Netherlands, 2003.

[31] Barton, Steve; Pierce, Garrett; Stroud, Daryl.: "Changing Selection Concepts: True Optimization of Drill Bits with Latest Generation Rotary Steerable Systems". SPE 124865, presented at SPE Annual Technical Conference and Exhibition, New Orleans, Louisiana, 4−7 October 2009.

[32] Stroud, D., Russell, M., and Peach, S.: "Development of the Industry's First Slimhole Point-the Bit Rotary Steerable System," paper SPE 84449 presented at the SPE Annual Technical Conference and Exhibition, Denver, Colorado, USA, 5−8 October, 2003.

[33] Chengru, Z.: "Elastic stability theory", Sichuan people's publishing house, 1981, Chengdu, P60-62.

[34] Jin Baozhen, Yang Wude, Zhu Baohua.: "Structural Mechanics", People's education publishing house, 1979, Beijing, P316-322.

[35] Ding Chongwen.: " Ordinary Differential Equation", Xia Men University Press, May 2006, P182-188.

[36] Fan Yingchuan.: "Advanced Mathematics", People's Education Press, 1978, Beijing.

[37] Hawkins, R., Jones, S., O'Connor, J., and Sugiura, J.: "Design, Development and Field Testing of a High Dogleg Slim-Hole Rotary Steerable System". SPE 163472, presented at the SPE/IADC Drilling Conference, 5-7 March, Amsterdam, the Netherlands, 2013.

[38] Timoshenko, S., Gaelic, J.: "Theory of Elastic Stability", (McGraw-Hill), second edition, translator Zhang Fufan, Beijing Science Press, 1965, P63-66, P71-73.